MASTER THESIS

Lykke Rasmussen

Calibrating the local volatility model

- an implicit finite difference approach

Internal superviser: Rolf Poulsen, University of Copenhagen
External superviser: Brian Norsk Huge, Danske Bank

March 1, 2012

Abstract

This thesis describes a method for calibrating the local volatility surface from a finite set of observed European-style option quotes. The method is originally proposed by Andreasen and Huge in their award winning article *Volatility Interpolation* from 2011. The implementation of the method and its underlying theory is described thoroughly in this thesis and numerically experiments are reported subsequently.

Resumé

Denne afhandling beskriver en metode til kalibrering af den lokale volatilitets overflade ud fra et endeligt sæt af markedspriser for europæiske optioner. Metoden er oprindeligt udviklet af Andreasen and Huge og beskrevet i deres award vindende artikel *Volatility Interpolation* fra 2011. Implementeringen af metoden og dens underliggende teori bliver i denne afhandling grundigt beskrevet og numeriske eksperimenter beskrives afslutningsvist.

Contents

1 Introduction

The ongoing search, within the quantitative finance discipline, for a pricing routine which improves in correlation to the aim:

> *Do it quickly, cheaply and in small memory.*
>
> - Press, Teukolsky, Vetterling, and Flannery (2007).

led Andreasen and Huge to the discovery, that the solution to the implicit finite difference discretisation of the Dupire forward equation [1] - with a time-independent volatility parameter - is a set of arbitrage free call prices, unconditional on the step size in the underlying mesh.

This discovery has formed the basis of a new approach to calibrating the local volatility surface to a set of discrete market quotes, which shifts the focus from convergence to stability and robustness. The method is presented in the article *Volatility Interpolation* published in 2011 by Andreasen and Huge.

Traditional finite difference based methods for calibrating the local volatility surface relies on call prices, given as the solution to a finite difference discretisation of the continuous time PDE specified by the model. These prices are for the traditional second-order schemes only arbitrage free when the discrete approximation converges towards the continuous time PDE. Hence, when the step size in the underlying grid approaches zero which is a computationally costly procedure. The focus has therefore traditionally been on how to increase the speed of this convergence.

The method presented by Andreasen and Huge challenges this traditional approach by using a first-order scheme for the continuous Dupire forward PDE and replacing the local volatility function with a piecewise constant volatility proxy, which is time-independent between the observable maturities. It can then be proved - using the *arbitrage discovery* - that the calibrated call surface obtained by this discrete set-up is arbitrage free, independent of the step size in the underlying grid. Thus, Andreasen and Huge does not have to worry about convergence or the speed of it.

The convexity in strike and slope in expiry of the calibrated call surface can then be used to obtain the local volatility function through the simple discretisation of the Dupire forward equation. The derivation of this equation

[1] See equation (11).

along with a description of the continuous time framework is given in section 3.

Section 5 of this thesis examines the details of the implementation of the method presented by Andreasen and Huge. Section 6 is focused on verifying the theoretical results regarding absence of arbitrage the method relies on.

According to the authors Andreasen and Huge, should this method be both fast and robust, as a coarse grid can be used for the method without introducing arbitrage to the call surface, and without introducing discontinuities or spikes in the local volatility surface. This claim will be tested through a 'C++' implementation of the method in the end of this thesis.

> *The point is we don't care about convergence - we care about an efficient, arbitrage-free way of getting prices across all strikes and expiries from a set of discrete market quotes.*
>
> - Jesper Andreasen 2012.

2 Model Warm-Up

Options and other financial derivatives are traded at markets which can be divided into two main categories:

- exchange-traded markets.
- over-the-counter markets.

Standardized contracts, such as vanilla options, are publicly traded at exchanges while contracts with more complex features usually are traded over-the-counter.

The value of these contracts can either be given as the arbitrage-free price or - for the exchange traded options - as the observed market price. The arbitrage-free price is derived using a pricing model which must ensure consistency[2] between the theoretical prices and the observed market prices.

2.1 Black-Scholes and his shortcommings

The classical - and ideal - choice for a pricing model is the Black-Scholes-Merton model developed in the early 1970s presented in the paper "*The Pricing of Options and Corporate Liabilities*". This model assumes that the price of a non-dividend paying stock S has a lognormal distribution with dynamics given by a geometric Brownian motion:

$$S(t) = \mu S(t)dt + \sigma S(t)dW(t)$$

where $W(t)$ is a Wiener process under the objective measure.

In order to obtain consistency between the market and the pricing model, the latter is initially *calibrated* to the market. That is, the set of unknown parameters of the model is specified such that the theoretical prices given by the model resembles the prices observed in the market for a given set of option. For this, and pricing in general, the risk-neutral price process for the underlying asset is needed:

$$S(t) = rS(t)dt + \sigma S(t)dW^Q(t)$$

[2]Consistency in the sense that no arbitrage possibilities are available in the market.

where $W^Q(t)$ is the Wiener process under the risk-neutral measure and r is the short rate.

The only one of these parameters: μ, σ, r, that cannot be directly observed in the market is the volatility of the underlying stock price σ[3]. This parameter can either be estimated from historical data for the stock price or it can be obtained by numerically inverting the B.S. formula to *back out* the volatility level consistent with a traded European-style option. The former is referred to as the *historical volatility* and the latter is referred to as the *implied volatility*: σ_{imp}.

> *Implied volatilities are used to monitor the market's opinion about the volatility of a particular stock. Whereas historical volatilities are backward looking, implied volatilities are forward looking.*
>
> - (Hull, 2008, p. 297).

The actual calibration is typically carried out on the basis of ATM and OTM European-style options, as these are the most liquid options traded in the market. Remark that the implied volatility of a European call option and a European put option are equivalent for a given strike and maturity, cf. (Hull, 2008, section 18.1). The implied volatilities should, in addition to this, be constant regardless of the strike and maturity of the option according to the Black-Scholes model. However, as illustrated in figure 1, this is not the case in practice.

In practice, when the implied volatility is illustrated as a function of the strike for a given maturity, the curve forms a:

- smile - for currency options - the implied volatility is low for ATM options an rises as the option moves either into the money or out of the money.
- skew or smirk - for equity or index options - the implied volatility is higher for the lower strike levels (deep OTM puts and deep ITM calls) than for the higher (deep OTM calls and deep ITM puts), as can be seen in figure 1.

Collectively these are referred to as the 'implied volatility smile' or just 'the volatility smile'.

[3]In this thesis, as in the finance litterature in general, both σ and σ^2 are referred to as the volatility parameter.

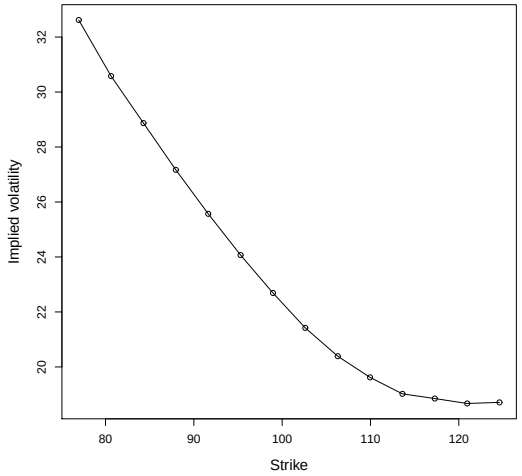

Figure 1: The implied volatility smile for European-style options on the SXE5 index with maturity 0.274 years. The data is taken from Andreasen and Huge (2011) and is given in appendix A in table 8.

The skew in the implied volatilities was not evident for equity options prior to 1987. But the stock market crash of October 1987

> *...appears to have increased the likelihood assigned by the financial markets to extreme stock market movements, in particular large downward movements...this change in view of stock market dynamics has resulted in a persistent, pronounced volatility smile in current options markets.*
>
> -(Andersen and Brotherton-Ratcliffe, 1997/98)

Hence, the market assigns a larger probability to large price-movements for European-style options with low strike levels than for those with high (ITM calls and OTM puts). Thus, the volatility implied by the quoted option prices is higher for options with low strikes.

The implied volatility does not only depend on the strike of the option, its shape also depends on the time to maturity. The smile becomes less pronounced, or less steep, as the maturity of the option increases. The isolated dependence of the maturity on the implied volatility is given by the 'implied volatility term structure'. The shape of this curve depend to some extend on the volatility levels for the maturities, if these are low the market generally

will expect an increase and vice versa.

The implied volatility smile and the implied volatility term structure can be combined into a *implied volatility surface* which provides a snapshot of the implied volatility as a function of strike and maturity. The shape of the volatility surface will change as the market changes its view on the prices for the European-style options.

2.2 Can he be fixed?

If one blindly uses the Blacks Scholes model for pricing without taking the shortcomming - regarding constants volatility - into account, one exposes him- or herself to unexpected volatiltiy risk [4].

Practitioners are able to account for this inaccuracy to some extent by using the implied volatility surface for a range of strikes and maturities to price European-style options. As Rebonato expressed it in 1999:

> The implied volatility is the wrong number to plug into the wrong formula to get the right price.

This technique is by some referred to as the *constant implied volatility approach* and it is per construction sufficient for pricing European-style options, but it is unsuited for pricing more complex structures.

Hence, one needs a more sophisticated model that can take the structure of the volatility surface into account. But with the added sophistication also comes an added computational burden, as these models has to be recalibrated to the market on a regular basis. Thus, despite the B.S. models imperfections it is still widely used amongst practitioners at least as an initial approximation because of its robustness and simplicity.

2.3 Expand

The supply of alternative models that takes the volatility smile and term structure into account has over the years grown to considerable size. It is outside the scope of this paper to present them all, but two of them have is of particular interest regarding the method by Andreasen and Huge (2011).

[4] This is not the only risk as the Black-Scholes model also suffers from other non-realistic assumptions besides constant volatility.

The simplest expansions is the *local volatility model* or the *generalized volatiltiy model*[5]. This model resembles the Black-Scholes model, apart from the parameters which are allowed to depend on the state of the underlying asset and the time.

The calibration method presented in Andreasen and Huge (2011) is developed for this model. The continuous time theory for the local volatiltiy model is therefore presented in the following section.

Andreasen and Huge use the local volatility function from this model as a part of the more sophisticated *local stochastic volatility* model which combines the local volatility model and the *stochastic volatility* model. The latter assumes that the volatility is driven by an additional stochastic process.

[5]This term is used by Björk.

3 Continuous time calibration - the local volatility model.

The continuous time framework for the local volatility model and the calibration of the local volatility function is presented in this section. The material is based on the work by Dupire (1993, 1994) and the continuous time arbitrage theory presented in Björk (2009, ch. 10).

3.1 The local volatility model

The local volatility model is an extension of the standard Black-Scholes model where the traded asset S is driven by a one-factor diffusion process with deterministic functions $\mu : [0,T] \times \mathbb{R}_+ \to \mathbb{R}$ and $\sigma : [0,T] \times \mathbb{R}_+ \to \mathbb{R}_+$, for the local rate of return and the volatility, respectively. Thus, the asset S satisfies the SDE:

$$\begin{aligned} dS(u) = \mu(u, S(u))S(u)du + \sigma(u, S(u))S(u)dW^P(u) \qquad & u \in (t,T] \\ S(t) = S_t > 0 \qquad & 0 \leq t. \end{aligned} \tag{1}$$

where W^P is a Wiener process under the objective measure P. Assume, as for the Black-Scholes model, that the economy is frictionless and assume w.l.o.g. that S is a non-dividend paying asset.

Assume absence of arbitrage in the primary market and let the numeraire be the money account with constant short rate r. Then there exists a martingale measure $Q \sim P$, according to the *first fundamental theorem of finance*, such that the Q-dynamics for S is given by:

$$\begin{aligned} dS(u) = rS(u)du + \sigma(u, S(u))S(u)dW^Q(u) \qquad & u \in (t,T] \\ S(t) = S > 0 \qquad & 0 \leq t. \end{aligned} \tag{2}$$

where W^Q is a Wiener process under the risk-neutral measure Q.

The primary market is then complete according to our *rules-of-thumb*[6], as the asset is only driven by one random source: the one-dimensional Wiener process W^P. Hence, the equivalent martingale measure, Q, is unique and the measure transformation is obtained from a *Girsanov* transformation.

[6]See Björk (2009, Meta-thm. 8.3.1) or the result in Björk (2009, thm. 8.3).

Let the unique arbitrage free price process for a simple T-claim: $\mathcal{X} = \Phi(S(T))$, be given by $\Pi(t, \mathcal{X}) = F(t, S(t))$. Where the function F either can be determined by the *risk neutral valuation formula*:

$$\begin{aligned} F(t,s) &= e^{-r(T-t)} E^Q \left[\mathcal{X} \mid \mathbb{F}_t^{W^Q} \right] \\ &\overset{(\diamond)}{=} e^{-r(T-t)} E^Q \left[\mathcal{X} \mid S(t) = s \right] \quad t \in [0,T] \end{aligned} \tag{3}$$

($\diamond$) The parameters, r and σ, are adapted to the filtration $\{\mathbb{F}_t^{W^Q}\}_{t \geq 0}$ generated by the Q-Wiener process. Thus, S is a Markov process.

or as the solution to the following *boundary value problem*[7] in the domain: $[0,T] \times \mathbb{R}_+$:

$$\begin{aligned} \frac{\partial F}{\partial t}(t,s) + rs\frac{\partial F}{\partial s}(t,s) + \frac{1}{2}s^2\sigma^2(t,s)\frac{\partial^2 F}{\partial s^2}(t,s) - rF(t,s) = 0 \\ F(T,s) = \Phi(s) \end{aligned} \tag{4}$$

3.2 CALIBRATING THE LOCAL VOLATILITY FUNCTION

Calibration of the local volatility model consists of adjusting the parameters of the model until the theoretical prices - usually European call prices for a range of strikes and maturities - approximately matches the observed prices[8].

The European call option with strike K and maturity T is a simple T-claim with payoff function: $\mathcal{X} = (S(T) - K)^+$. The arbitrage free price process, $C(t, s; T, K)$, for this derivative can then according to the previous section be determined by either the *risk neutral valuation formula*:

$$C(t, s : T, K) = e^{-r(T-t)} E^Q \left[(S(T) - K)^+ | S(t) = s \right] \qquad t \in [0,T] \tag{5}$$

or as the solution to the *boundary value problem* with terminal condition given by the payoff function above:

$$\begin{aligned} \frac{\partial C}{\partial t}(t,s) + rs\frac{\partial C}{\partial S}(t,s) + \frac{1}{2}s^2\sigma^2(t,s)\frac{\partial^2 C}{\partial s^2}(t,s) - rC(t,s) = 0 \\ C(T,S) = (S-K)^+ \end{aligned} \tag{6}$$

where the parameters T and K have been suppressed. This PDE is also referred to as the *backward pricing PDE* as it is given in terms of the backward

[7] See Björk (2009, ch. 7) for the derivation of the no-arbitrage PDE for - what the author refers to as - the generalized Black Scholes model.

[8] Exactly how well these prices should match is discussed in section 4.3 below.

variables (t, s).

Assume that the short rate r can be observed in the market. Then the calibration of the local volatility model is reduced to specifying the local volatility function: $\sigma(t, s)$. Remark that the local volatility functions under the P- and Q-measure are equivalent, as the Girsanov transformation maintains the volatility parameter.

The issue here is that neither of these formulas for the theoretical price can be evaluated analytically. Thus, in practice a numerical method must be chosen in order to solve the pricing problem. There are two obvious choices for this:

- Finite difference methods for solving the pricing PDE.
- Monte Carlo simulation for estimating the expectation in the risk neutral valuation formula.

As a rule-of-thumb the latter method is the computationally most efficient[9] when dealing with problems of dimension four or higher. For lower dimensional problems, such as the one dimensional problem for the local voaltility model, the finite difference method will is the obvious choice.

Solving the boundary value problem (6) for a single call option, using a finite difference method, require calculation of call prices $C(t_j, s_i; T, K)$ for all points (t_j, s_i) in a rectangular grid starting from $t_N = T$ down to $t_0 = t$, as illustrated in figure 2(a).

If instead the PDE where given in terms of the forward variables (T, K), the application of a finite difference method would yield a grid containing the current prices $C(t, s; T_j, K_i)$ for a range of call options with strikes and maturities corresponding to the grid-points (T_j, K_i). This is illustrated in figure 2(b). Thus, the calibration for a range of European options can be carried out much faster in a forward system.

The transformation from the backward PDE to a consistent forward PDE is described along the lines of Dupire (1994) in the section below.

[9] Fast and easy to implement.

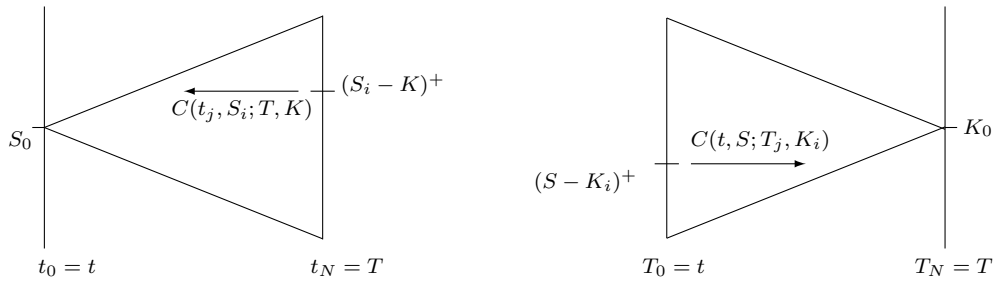

(a) The backward system

(b) The forward system

Figure 2: Illustration of the finite difference method applied to the backward and forward system, respectively.

3.3 The Dupire forward equation

The forward PDE consistent[10] with eqn. (6) can be derived along the lines of Dupire: *'Pricing and hedging with smiles'*, from 1994. The *Kolmogorov forward equation* and the relationship between the *surface* of European call prices and the *transition density*, is used as a central part of the derivation and are therefore initially introduced.

Proposition 1 (Kolmogorov forward equation). *Suppose that X is the solution to the SDE:*

$$dX(t) = \mu(t, X(t))dt + \sigma(t, X(t))dW(t)$$

Then the transition density $\varphi(s, y; t, x)$ of $x(t) = x$ given $x(s) = y$ will satisfy the 'Kolmogorov forward equation'

$$\frac{\partial}{\partial t}\varphi(s, y; t, x) = -\frac{\partial}{\partial x}\left[\mu(t, x)\varphi(s, y; t, x)\right] + \frac{1}{2}\frac{\partial^2}{\partial x^2}\left[\sigma^2(t, x)\varphi(s, y; t, x)\right]$$
$$\varphi(s, y; t, x) \to \delta_y \text{ as } t \downarrow s, \ (t, x) \in (s, T) \times \mathbb{R}$$

where δ_y is the dirac function:

$$\delta_y(x) = \begin{cases} +\infty & y = x \\ 0 & y \neq x \end{cases}, \qquad \int_{-\infty}^{\infty} \delta_y(x)dx = 1$$

[10] Consistent in the sense that they agree on the price of a given European call option.

Recall the SDE for the asset S under the Q-measure given in eqn. (2) and let the corresponding risk neutral transition density of $S(T) = S$ given $S(t) = s$ be denoted $\varphi(t, s; T, S)$ with backward and forward variables given as (t, s) and (T, S), respectively. According to proposition 1 the density φ will then satisfy:

$$\frac{\partial}{\partial t}\varphi(t,s;T,S) = -\frac{\partial}{\partial S}\left[rS\varphi(t,s;T,S)\right] + \frac{1}{2}\frac{\partial^2}{\partial S^2}\left[\sigma^2(T,S)S^2\varphi(t,s;T,S)\right]$$
$$\varphi(t,s;T,S) \to \delta_s(S) \; as \; T \downarrow t, \qquad (T,S) \in (t,\bar{T}) \times \mathbb{R}_+ \quad (7)$$

The risk neutral transition density, $\varphi(t, S; T, K)$, can be deduced from a range of European call options with different strike levels for a fixed maturity T and a current spot S. This is achieved by differentiating the risk neutral valuation formula for the European call option twice with respect to the strike as established below. This result was first derived by Breeden and Litzenberg in 1978.

Recall from eqn. (5) the arbitrage free price at time t for a European call option with strike K and maturity T:

$$\begin{aligned} C(t,s;T,K) &= e^{-r(T-t)}E^Q\left[(S(T)-K)^+ \mid S(t)=s\right] \qquad t \in [0,T] \\ &= e^{-r(T-t)}\int_K^\infty (S-K)\,\varphi(t,s;T,S)dS \end{aligned} \quad (8)$$

Differentiating this formula once with respect to K yields:

$$\begin{aligned} & e^{r(T-t)}\frac{\partial C}{\partial K}(t,s;T,K) \\ &= \frac{\partial}{\partial K}\left(\int_K^\infty S\varphi(t,s;T,S)dS - \int_K^\infty K\varphi(t,s;T,S)dS\right) \\ &= \lim_{u\to\infty}\left(-\frac{\partial}{\partial K}\int_u^K S\varphi(t,s;T,S)dS + \frac{\partial}{\partial K}K\int_u^K \varphi(t,s;T,S)dS\right) \\ &\overset{FTC}{=} \lim_{u\to\infty}\left(-K\varphi(t,s;T,K) + \int_u^K \varphi(t,s;T,S)dS + K\varphi(t,s;T,K)\right) \\ &= \lim_{u\to\infty}\left(\int_K^u \varphi(t,s;T,S)dS\right) \\ &= -\int_K^\infty \varphi(t,s;T,S)dS. \end{aligned} \quad (9)$$

and differentiating once again with respect to K:

$$\begin{aligned} e^{r(T-t)}\frac{\partial^2 C}{\partial K^2}(t,s;T,K) &= -\frac{\partial}{\partial K}\int_K^\infty \varphi(t,s;T,S)dS \\ &= \lim_{u\to\infty}\left(\frac{\partial}{\partial K}\int_u^K \varphi(t,s;T,S)dS\right) \\ &= \lim_{u\to\infty}\varphi(t,s;T,K) = \varphi(t,s;T,K) \end{aligned} \tag{10}$$

where $\varphi(t,s;T,K) \to \delta_s(K)$ for $T \downarrow t$. The correspondence between these transition densities and the risk-neutral diffusion process for the underlying asset S is uniquely given under some technical assumptions, cf. Dupire (1994).

The forward PDE consistent with the backward PDE, for a given European call option, given in eqn. (6) can then be derived by means of the two results above. In order to be able to apply the first result: *the Kolmogorov forward equation*, the European call price from eqn. (8) is initially differentiated w.r.t the maturity T:

$$\begin{aligned} \frac{\partial C}{\partial T}(t,s;T,K) =& \frac{\partial}{\partial T}\left[e^{-r(T-t)}\int_K^\infty (S-K)\varphi(t,s;T,S)dS\right] \\ \overset{\substack{Leibniz\\ rule}}{=}& -re^{-r(T-t)}\int_K^\infty (S-K)\varphi(t,s;T,S)dS \\ &+ e^{-r(T-t)}\int_K^\infty (S-K)\frac{\partial\varphi}{\partial T}(t,s;T,S)dS \\ \overset{eqn.\ (7)}{=}& -rC(t,s;T,K) \\ &- re^{-r(T-t)}\int_K^\infty (S-K)\frac{\partial}{\partial S}\left[S\varphi(t,s;T,S)\right]dS \\ &+ \frac{1}{2}e^{-r(T-t)}\int_K^\infty (S-K)\frac{\partial^2}{\partial S^2}\left[\sigma^2(T,S)S^2\varphi(t,s;T,S)\right]dS \end{aligned}$$

Both of these integrals can be evaluated by means of ordinary *integration by parts*. Assume in the calculations below that $\varphi(t,s;T,S)$ and $\frac{\partial}{\partial S}\varphi(t,s;T,S)$ tend to zero sufficiently fast as S tends to ∞, such that those terms below - in which they are involved - vanish.

The evaluation of the first integral yields:

$$\begin{aligned} f(S) &= \frac{\partial}{\partial S}\left[S\varphi(t,s;T,S)\right] & F(S) &= S\varphi(t,s;T,S) \\ g(S) &= (S-K) & g'(S) &= 1 \end{aligned}$$

$$\begin{aligned}
&\int_K^\infty (S-K)\frac{\partial}{\partial S}\left[S\varphi(t,s;T,S)\right]dS \\
&\qquad = \left[F(S)g(S)\right]_K^\infty - \int_K^\infty F(S)g'(S)dS \\
&\qquad = \left[S\varphi(t,s;T,S)(S-K)\right]_K^\infty - \int_K^\infty \left[S\varphi(t,s;T,S)\right]1dS \\
&\qquad = \lim_{u\to\infty}\left[u\varphi(t,s;T,u)(u-K)\right] - \int_K^\infty S\varphi(t,s;T,S)dS \\
&\qquad = -\int_K^\infty S\varphi(t,s;T,S)dS \\
&\qquad = -\left(\int_K^\infty (S-K)\varphi(t,s;T,S)dS + \int_K^\infty K\varphi(t,s;T,S)dS\right) \\
&\qquad = -e^{r(T-t)}\left(C(t,s;T,K) - K\frac{\partial C}{\partial K}(t,s;T,K)\right)
\end{aligned}$$

where the last equality follows from the results given in eqn. (8) and (9).

The evaluation of the second integral yields:

$$\begin{aligned}
f(S) &= \frac{\partial^2}{\partial S^2}\left[\sigma^2(T,S)S^2\varphi(t,s;T,S)\right] & F(S) &= \frac{\partial}{\partial S}\left[\sigma^2(T,S)S^2\varphi(t,s;T,S)\right] \\
g(S) &= (S-K) & g'(S) &= 1
\end{aligned}$$

$$\begin{aligned}
&\int_K^\infty (S-K)\frac{\partial^2}{\partial S^2}\left[\sigma^2(T,S)S^2\varphi(t,s;T,S)\right]dS \\
&\qquad = \left[F(S)g(S)\right]_K^\infty - \int_K^\infty F(S)g'(S)dS \\
&\qquad = \left[\frac{\partial}{\partial S}\left[\sigma^2(T,S)S^2\varphi(t,s;T,S)\right](S-K)\right]_K^\infty - \int_K^\infty \frac{\partial}{\partial S}\left[\cdots\right]1dS \\
&\qquad = \lim_{u\to\infty}\frac{\partial}{\partial S}\left[\sigma^2(T,u)u^2\varphi(t,s;T,u)\right](u-K) - \int_K^\infty \frac{\partial}{\partial S}\left[\cdots\right]dS \\
&\qquad = -\int_K^\infty \frac{\partial}{\partial S}\left[\sigma^2(T,S)S^2\varphi(t,s;T,S)\right]dS \\
&\qquad = -\left[\sigma^2(T,S)S^2\varphi(t,s;T,S)\right]_K^\infty \\
&\qquad = -\left(\lim_{u\to\infty}\left[\sigma^2(T,u)u^2\varphi(t,s;T,u)\right] - \sigma^2(T,K)K^2\varphi(t,s;T,K)\right) \\
&\qquad = \sigma^2(T,K)K^2\varphi(t,s;T,K).
\end{aligned}$$

The terms can then be collected:

$$\begin{aligned}\frac{\partial C}{\partial T}(t,s;T,K) =& -rC(t,s;T,K)\\ &+re^{-r(T-t)}e^{r(T-t)}\left(C(t,s;T,K)-K\frac{\partial C}{\partial K}(t,s;T,K)\right)\\ &+\frac{1}{2}e^{-r(T-t)}\sigma^2(T,K)K^2\varphi(t,s;T,K)\\ &=-rK\frac{\partial C}{\partial K}(t,s;T,K)\\ &+\frac{1}{2}e^{-r(T-t)}\sigma^2(T,K)K^2\varphi(t,s;T,K)\end{aligned}$$

and the transition density can be substituted using eqn. (10):

$$\begin{aligned}\frac{\partial C}{\partial T}(T,K) &= \frac{1}{2}\sigma^2(T,K)K^2\frac{\partial^2 C}{\partial K^2}(T,K)-rK\frac{\partial C}{\partial K}(T,K)\\ \Leftrightarrow 0 &= -\frac{\partial C}{\partial T}(T,K)+\frac{1}{2}\sigma^2(T,K)K^2\frac{\partial^2 C}{\partial K^2}(T,K)-rK\frac{\partial C}{\partial K}(T,K)\end{aligned} \tag{11}$$

where the current time t and the spot $S(t)$ has been suppressed.

This is the forward PDE consistent with the backward PDE given in eqn. (6) and this equation is referred to as the *Dupire forward equation.*

3.4 Calibrating the local volatility function in terms of Dupire

If a continuum of arbitrage free market prices for European-style options were available, then the local volatility function could be uniquely determined from the slope in expiry and convexity in strike of these prices through the Dupire equation:

$$\sigma^2(T,K) = 2\frac{\frac{\partial C}{\partial T}(t,s;T,K)+rK\frac{\partial C}{\partial K}(t,s;T,K)}{K^2\frac{\partial^2 C}{\partial K^2}(t,s;T,K)} \tag{12}$$

But, as previously mentioned, there are only a limited number of European option quotes available in practice for a given underlying asset. The dataset from Andreasen and Huge (2011) on the SX5E index, for instance, consists of 155 mid-point quotes dispersed over 12 maturities and 26 strike levels.

Thus, in practice, the derivatives in eqn. (12) can obviously not be evaluated directly and the number of observed option quotes is too limited to

obtain a reasonable result from a direct finite difference discretization.

Instead of trying to evaluate eqn. (12) directly, take one step back to the original form of the Dupire forward equation in (11). The initial boundary value problem corresponding to this forward PDE on the domain:$[t, \bar{T}] \times \mathbb{R}_+$, is given by:

$$-\frac{\partial C}{\partial T}(T,K) + \frac{1}{2}\sigma^2(T,K)K^2\frac{\partial^2 C}{\partial K^2}(T,K) - rK\frac{\partial C}{\partial K}(T,K) = 0 \qquad (13)$$
$$C(t,s;0,K) = (s-K)^+$$

This IBVP can be discretised and solved forward in time T by using an appropriate finite difference method. Thereby a dense grid consisting of arbitrage free call prices for a range of strikes and maturities would be obtained, as described in section 3.2. It would then be possible to approximate the right-hand-side of eqn. (12) by finite differences using this *surface* of call values.

The only obvious problem with this approach is, that the volatility function, $\sigma^2(T,K)$, in the IBVP is unknown. Various techniques to overcome this problem have been proposed and a few of these is outlined in the following section.

4 Previous attempts of retrieving the local volatility function.

The issue of accurately calibrating the local volatility function to a limited number of market observations - with as low computational and storage costs as possible - has been investigated in numerous papers. The resulting procedures can be divided into two main approaches:

- Direct calibration of the local volatility function to the data, where assumptions on the functional form of the volatility parameter have to be made in order to secure a unique solution.
- Indirect fitting of the local volatility parameter to an arbitrage free surface of European call prices - or implied volatilities - consistent with the data through eqn. (12). As the local volatility function depends on the derivatives of these call prices, the surface ought to be smooth in order to obtain a reliable result. Several methods for constructing such a call surface is described in the litterature and these can also be divided into two main categories: parametric and non-parametric.

In this section a few examples of these approaches are outlined.

4.1 Full-scale optimization

An example of a direct calibration method is given in the article *Reconstructing The Unknown Local Volatility Function* by Coleman, Li, and Verma (1998).

The authors propose to approximate the local volatility function by a cubic spline: $\sigma(t,s) \approx c(t,s)$, as splines are often used as an approximation of smooth curves and surfaces. An examination of the local volatility function in the region of interest: $S \times T : (0,\infty) \times (0,\bar{T})$, justifies this choice.

For this cubic spline a number of fixed spline knots $\{\bar{s}_i, \bar{t}_i\}_{i=1}^{p}$ in the region of interest is chosen. The determination of the number and location of these spline knots is not trivial and the calibrated volatility function will to some extend depend on this.

The cubic spline can then be uniquely determined by a fixed end condition and the value of the spline at the chosen knots:

$$c(\bar{s}_i, \bar{t}_i) = \bar{\sigma}_i, \quad i = 1, \ldots, p$$

The values $\bar{\sigma_i}$ are determined by calibrating the local volatiltiy model with volatility parameter $c(\bar{s_i}, \bar{t_i})$ to N observed option prices.

The calibration is carried out by solving the minimization problem:

$$\min_{\bar{\sigma} \in \mathbb{R}^p} \frac{1}{2} \sum_{j=1}^{N} w_j \left[v_j(K_j, T_j; c(s,t;\bar{\sigma})) - \bar{v_j} \right]^2$$

$$s.t. \quad l \leq \bar{\sigma} \leq u$$

where $\bar{v_j}$ is the j'th observed market price for an European call option with strike K_j and maturity T_j and $v_j(K_j, T_j; c(s,t;\bar{\sigma}))$ is the corresponding theoretical price computed in the model. The weights w_j allow for adjusting the influence of different observations or computed values.

As noted in section 3.2 there does not exist a closed form solution for the price of a European call option in the local volatility model and the prices v_j must therefore be calculated by a numerical method. In order to obtain the prices for all the observed strikes and maturities an entire surface of call prices must be numerically determined for each iteration. Thus, this global optimization procedure is highly expensive computational- and storage- wise.

4.2 The SABR model

The downside to the direct method presented above is primarily the computational effort needed to calculate the European call prices numerically in the local volatility model. This problem can for instance be overcome by *transferring* the calculation of the option prices to a model where an analytical formula for the European call price or - as in the example below - the implied volatility - is available.

Popular choices for this *intermediate* model are, amongst others, the stochastic models: Heston and SABR, where (semi-) analytical formulas are available. An example of an indirect parametric approach based on the SABR model is found in *Using SABR model to produce smooth local volatility surfaces* by Sepp (2007).

The SABR (Stochastic, Alpha, Beta, Rho) model assumes that the dynamics of the forward asset price $F(t)$ and its instantaneous volatility $\alpha(t)$ are given

by the SDE's:

$$dF(t) = \alpha(t)F^{\beta}(t)dW^{f}(t), \quad F(0) = F,$$
$$d\alpha(t) = \nu\alpha(t)dW^{\alpha}(t), \quad \alpha(0) = \alpha.$$

where the Wiener processes are correlated $dW^{f}(t) \cdot dW^{\alpha}(t) = \rho$, the parameter ν is the *vol-of-vol* and β is a constant.

An analytical formula for the implied volatility is available in the SABR model and this formula is used for calibrating the model to the market data for each of the observable maturities separately. Thus, the SABR model is used for capturing the volatility smile observed in the market for each of the available maturities.

The calibration is carried out by minimizing the squared differences between the market data and the implied volatiltiy approximated by the model, see Sepp (2007, eqn. (2.1)). Thus, a set of parameters is obtained for each of the n maturities:

$$(\alpha^{*}(T_j), \nu^{*}(T_j), \rho^{*}(T_j))_{j=1,\ldots,n.}$$

In order to produce a smooth surface, these separate models need to be combined across all maturities in a way that does not introduce arbitrage. The authors propose to do this by polynomial interpolation of the parameters ν and ρ in the time direction and subsequently estimating the values of α from these.

This part could be avoided if an extension of the SABR model with time-dependent parameters where used instead, such that the calibration in the strike and time direction could be carried out simultaneously. The main disadvantage of such a model would be the increased computational time stemming from the optimization procedure being expanded from n smiles to an entire surface. Thus, in practice this model is avoided as the *greed for speed* is often the predominant consideration.

The final step in the procedure is to determine the local volatility function from the calibrated surface of implied volatilities. This can be carried out through either eqn. (12) - in conjunction with the Black Scholes formula - or, alternatively, through the extension of eqn. (12) given directly in terms of the implied volatilities[11].

[11] This result is given in Gatheral (2006, eqn. (1.10)).

Compared to the direct method from the previous section, this method is computationally faster but also more restrictive with regards to the assumptions made on the dynamics of the forward and its diffusion term.

4.3 Implied-density approach

A less restrictive non-parametric indirect approach is presented in the article *Recovering the probability Distributions from Option Prices* by Jackwerth and Rubinstein (1996).

The method is build upon the article *Implied binomial trees* by Mark Rubinstein (1994). Who presents a method for deriving the risk-neutral probability distribution of the underlying asset from observed European-style option prices in the binomial tree framework.

Jackwerth and Rubinstein (1996) further develop this technique imposing a smoothness criterion on the probability distribution.

Hence, the risk-neutral probabilities P_j of the underlying asset being at state j at time T is calibrated to the N observed prices - for European-style options with maturity T - by optimizing the merit-function:

$$\min_{\bar{P}} \sum_{j=1}^{m} \left(\frac{\partial^2 P_j}{\partial K_j^2} \right)^2$$

subject to additional regulative constraints, including that each of the observed call prices must be equal to the current value of the expected payoff in the tree:

$$\hat{C}(T, K_i) = r^{-n} \left(\sum_{j=1}^{m} P_j \left(S_j - K_i \right)^+ \right).$$

This merit-function is then rewritten by using the Breeden-Litzenberger result derived in section 3.3: $P_j = \frac{\partial^2 C_j}{\partial K_j^2}$, and replacing the derivative by its finite difference approximation:

$$\min_{C(T,\bar{K})} \sum_{j=1}^{m} \left(C(T, K_{j-2}) - 4C(T, K_{j-1}) + 6C(T, K_j) - 4C(T, K_{j+1}) + C(T, K_{j+2}) \right)^2$$

$$\text{s.t. } C(T, K_j) = \hat{C}(T, K_i) \quad \text{whenever } K_j = K_i \quad \text{for } i = 1, \ldots, N.$$

where the constraint secures that the generated call prices exactly matches the market prices for all observed strikes. The local volatility smile for this

maturity T it then retrieved from these calibrated call prices through equation (12).

This procedure can be repeated for each of the observed maturities, as where done for the SABR model. But in this case there is no trivial approach for arbitrage-consistent interpolation of call prices between these maturities, according to Andreasen and Huge (2011).

Furthermore, remark the constraint securing that the observed option prices is exactly matched by the estimated call prices. This constraint separates this method from the other two described above.

There is a dispute in the literature of whether or not this characteristic is a desirable feature. Andreasen and Huge (2011) argues that not exactly matching all the observed option prices is one of the drawbacks of the first two methods described.

Coleman et al. on the other hand argue, that this should not be the only objective when calibrating the local volatility function. Firstly, a function which only has to match the observed prices can be very different from the true local volatility function. Secondly, the observed European option prices is also associated with uncertainty because of the bid-ask spread.

4.4 Implicit finite difference based approach

Andreasen and Huge present an alternative method, which combines some of the ideas presented above, in their article *Volatility Interpolation* from 2011.

They take the forward IBVP given in eqn. (13), as a starting point of their method. Recall that the forward PDE included in this IBVP was derived based on the Breeden-Litzenberger result which also were used in the *Implied-density approach* described above.

The forward PDE is then initially discretised by a fully implicit finite difference method and the local volatility function is replaced by an approximation as in the *full-scale optimization* method. This *volatility proxy* is given by a piecewise time-independent and piecewise constant function which is uniquely determined from the volatility levels a_{ij}.

The method then consists of calibrating this volatility proxy to the market data for each of observed maturities and thereby also deriving a set of call prices for these maturities. This approach is similar to the one used for the SABR model.

The interpolation between the observed maturities is afterwards carried out by solving one time step in the implicit finite difference method. The surface of call prices obtained by this, is then used to derive the original local volatility function trough a finite difference discretisation of eqn. (12).

The details of this technique is studied in section 5 and it is shown in section 6 that the interpolation technique does not introduce arbitrage to the surface of call prices.

5 Discrete time calibration

The calibration technique presented in the Andreasen and Huge (2011) is described in detail in this section. The method consists of two main steps:

- Calibration of an arbitrage free surface of European call prices.
- Derivation of the local volatility function from this call surface.

Assume in the following that the short rate, r, is equal to zero as in the article.

The first part is based in a finite difference discretisation of the IBVP based on the Dupire forward PDE for a European call option with maturity T strike K on the domain:$[t, \bar{T}] \times \mathbb{R}_+$, given in eqn. (13):

$$-\frac{\partial C}{\partial T}(T,K) + \frac{1}{2}\sigma^2(T,K)K^2\frac{\partial^2 C}{\partial K^2}(T,K) = 0 \qquad (14)$$
$$C(t,s;0,K)) = (s-K)^+$$

The second part consists of evaluating the finite difference approximation of the corresponding Dupire formula for the local volatility function:

$$\sigma^2(T,K) = 2\frac{\frac{\partial C}{\partial T}(t,s;T,K)}{K^2\frac{\partial^2 C}{\partial K^2}(t,s;T,K)}. \qquad (15)$$

Suppose that a set of discrete mid-quotes is available in the market at time t for European-style options written on a given underlying asset S:

$$c(\tau_i, K_{ij}) \quad i = 1,\ldots,n, \quad ij = 1,\ldots,m_i.$$

The index ij symbolises that the number of available quotes depends on the given maturity τ_i. Let the current spot price of the underlying asset be denoted s.

5.1 Discretization of the initial boundary value problem

The finite difference scheme chosen for discretising the IBVP above consists of a time discretisation part and a space discretisation part which are given below.

5.1.1 - The time domain

Initially the notation from the continuous time framework is eased by a coordinate transformation of the time variable: $\tau = T - t$, such that the forward equation from now on is given in terms of the time-to-maturity on the domain: $[0, \bar{\tau}] \times \mathbb{R}_+$:

$$-\frac{\partial C}{\partial \tau}(\tau, K) + \frac{1}{2}\sigma^2(\tau + t, K)K^2\frac{\partial^2 C}{\partial K^2}(\tau, K) = 0 \qquad (16)$$
$$C(0, K) = (s - K)^+$$

where $C(\tau, K) = C(t, s; T, K)$ and $\bar{\tau} = \bar{T} - t$.

The time domain: $[0, \bar{\tau}]$, is discretised into a non-uniform set of grid points corresponding to the observable maturities at time t:

$$0 = \tau_0 < \tau_1 < \cdots < \tau_n = \bar{\tau}$$

with backward increments given by: $\Delta\tau_i = \tau_i - \tau_{i-1}$ for $i = 1, \ldots, n$.

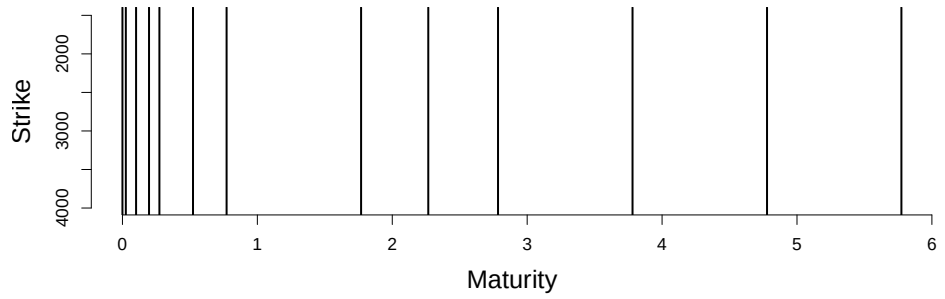

Figure 3: The semi-discrete grid with a continuum of points in the strike direction for each available maturity in the dataset given in Andreasen and Huge (2011), see appendix A.

Suppose that the local volatility function, $\sigma^2(\tau + t, K)$, is independent of time for each of the sub-periods formed by the observed time-to-maturities:

$$(\tau_{i-1}, \tau_i], \quad i = 1, \ldots, n.$$

The local volatility function, $\sigma^2(\cdot)$[12], can then be replaced by n proxy's: $\vartheta_i(K)$, formed as piecewise constant functions:

$$\vartheta_i(K) = \begin{cases} a_1 & K \leq b_1 \\ a_{ij} & b_{ij-1} < K \leq b_{ij} \quad ij = 2, \dots m_i - 1 \\ a_{m_i} & b_{m_i-1} < K \end{cases}$$

where the b_{ij}'s are given as the mid-points of the observed strike levels for the given maturity τ_i:

$$b_{ij} = \frac{K_{ij+1} - K_{ij}}{2} \qquad ij = 1, \dots, m_i - 1$$

Thus, volatility proxy i is uniquely determined by m_i volatility levels, equal to the number of observed strike levels for maturity τ_i. An example of a set of proxy functions for three sub-periods can be seen in figure 4.

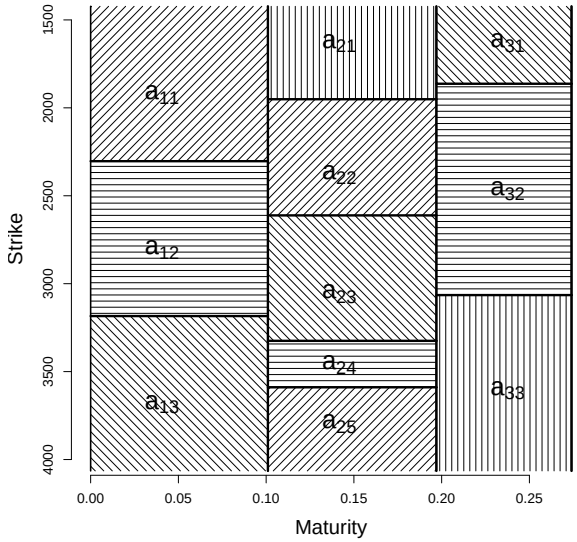

Figure 4: A set of piecewise constant volatility functions for each of the three sub-periods.

The difference scheme chosen as approximation for the time derivative in (16) determines the specific type of finite difference method used for the numerical evaluation.

[12]There seems to be some inconsistency in the article of whether $\sigma(\cdot)$ or $\sigma(\cdot)K$ should be replaced by the volatility proxy. But as the logarithmic transformation of the spatial coordinates in the section 7 is nicer for the first choice, this is used throughout this thesis.

A forward scheme yields an explicit method, a backward scheme yields an implicit method and a *half-and-half* combination of the two yields a Crank-Nicolson method.

The choice for *the pro's* would normally be the Crank-Nicolson method which is unconditionally stable[13] and second order accurate[14]. But according to Tavella and Randall (2000) this method may exhibit *undesirable qualities* - such as persistent oscillations or strange values - if the step size in the time dimension is very large.

In this setting, where the time steps are given according to the available data, the implicit method will be a better choice, as it does not exhibit the same sensitivity towards the step size. The cost of this additional stability is a step down to first order accuracy. But, as mentioned earlier, the convergence order is not a priority for the method considered here.

Let $\tilde{C}(\tau_i, K)$ - in short $\tilde{C}_i(K)$ - be the semi-discrete function approximating the exact solution, $C_\vartheta(\tau, K)$, to the IBVP given in eqn. (16) where the volatility parameter has been replaced with the proxy's. Thus, the partial differential difference equation (PDDE) governing this approximation is - for the implicit finite difference method - given by replacing the time derivative with a backward difference:

$$-\frac{\tilde{C}_i(K) - \tilde{C}_{i-1}(K)}{\Delta\tau_i} + \frac{1}{2}\vartheta_i^2(K)K^2\frac{\partial^2\hat{C}_i(K)}{\partial K^2} = 0$$

and the corresponding semi-discrete IBVP on the domain: $\{\tau_i\}_{i=0,\ldots,n} \times \mathbb{R}_+$, is given by:

$$\left[1 - \frac{1}{2}\Delta\tau_i\vartheta_i^2(K)K^2\frac{\partial^2}{\partial K^2}\right]\tilde{C}_i(K) = \tilde{C}_{i-1}(K) \quad i = 1, \ldots, n. \tag{17}$$
$$\tilde{C}_0(K) = (s - K)^+.$$

5.1.2 - The spatial domain

The spatial domain for the PDDE presented in the previous section: $K \in \mathbb{R}_+$, is semi-infinite and hence, cannot be approximated by a finite grid.

[13] An unconditional stable method is a method for which the stability of the solution does not depend on the step size in the underlying grid.

[14] The accuracy of a finite difference scheme is a measure for the speed of convergence towards the exact solution, when the step size in the underlying grid is decreased. The conditions for convergence are given by the *Lax equivalence theorem*, see Tavella and Randall (2000, p. 66).

Consequently this domain must initially be truncated to a finite interval: $[K_{min}, K_{max}]$, and a set of boundary conditions will account for the deleted portions.

The solution to the system is significantly influenced by the quality of the boundary conditions. If the boundary conditions creates a lot of oscillations, then the grid needs to be wider, in order keep the solution stable in the region of interest.

Hence, the exact values of the boundaries are determined through numerical experiments and will be examined in section 7.

The truncated spatial domain is then uniformly discretised independently of the observed data:

$$K_j = K_{min} + j\Delta K \quad \text{for } j = 0, \ldots, m.$$

where $\Delta K = (K_{max} - K_{min})/m$.

Figure 5 displays a grid for a domain discretised in the time-direction as well as the space direction.

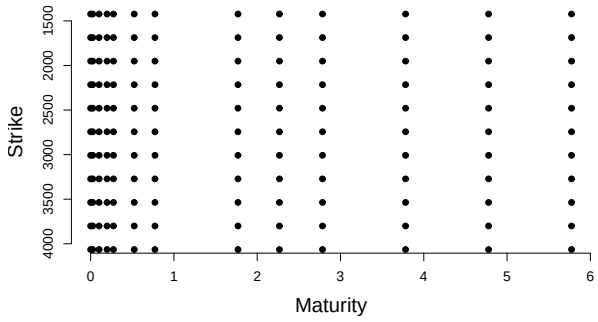

Figure 5: The fully discretised domain given by a grid with 10 strike levels for each maturity given in the dataset given in appendix A.

The boundary conditions applied to the lower boundary, K_{min}, and the upper boundary, K_{max}, stem from a look at the payoff function for a European call option given in terms of the strike level.

It seems reasonable from figure 6 to use Neumann conditions on the second order derivatives at the boundaries of the spatial domain:

$$\frac{\partial^2 C(\tau, K_{min})}{\partial K^2} = \frac{\partial^2 C(\tau, K_{max})}{\partial K^2} = 0$$

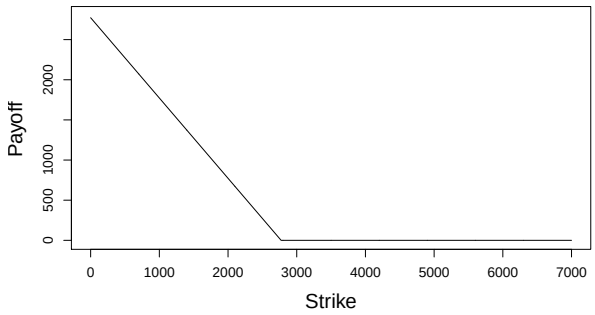

Figure 6: The payoff fucntion for a European call option in terms of the strike level for the current spot of the underlying: 2772.70.

In this case where the first order derivative w.r.t. the strike does not enter into the PDDE given in eqn. (17), these conditions are equivalent to assuming absorbing boundaries.

Now, let $\hat{C}(\tau_i, K_j)$ - in short $\hat{C}_{i,j}$ - be the discrete function approximating the the solution, $C(\tau, K)$, to the semi-discrete IBVP given in eqn. (17). The second order spatial derivative of this discrete function is approximated by a second order central difference:

$$-\frac{\hat{C}_i(K) - \hat{C}_{i-1}(K)}{\Delta\tau_i} + \frac{1}{2}\vartheta_i^2(K)K^2\frac{\hat{C}_{i,j-1} - 2\hat{C}_{i,j} + \hat{C}_{i,j+1}}{\Delta K^2} = 0$$

Hence, the fully discretized IBVP for the European call price: $\hat{C}(\tau_i, K_j)$, on the domain: $\{\tau_i\}_{i=0,\ldots,n} \times \{K_j\}_{j=0,\ldots,m}$, is given by:

$$\left[1 - \frac{1}{2}\Delta\tau_i\vartheta_i^2(K_j)K_j^2\delta_{KK}\right]\hat{C}_{i,j} = \hat{C}_{i-1,j} \quad i = 1,\ldots,n, \quad j = 1,\ldots,m-1. \tag{18}$$

$$\hat{C}_{0,j} = (s - K_j)^+ \qquad j = 0,\ldots,m. \tag{19}$$

$$\delta_{KK}\hat{C}_{i,0} = \delta_{KK}\hat{C}_{i,m} = 0 \qquad i = 1,\ldots,n. \tag{20}$$

where δ_{KK} is the central difference operator given by:

$$\delta_{yy}f(x_i, y_j) = \frac{1}{\Delta y^2}\left(f(x_i, y_{j+1}) - 2f(x_i, y_j) + f(x_i, y_{j-1})\right).$$

5.2 The calibration

The actual calibration part of the technique is based on the discretisation given above and consists of constructing a consistent arbitrage free call surface. This part is examined in this section.

5.2.1 The calibration set-up

The agreement between between the market data $\{c(\tau_i, K_{ij})\}_{i=1,\ldots,n.\ ij=1,\ldots,m_i.}$ and the theoretical prices given as the solution to the discrete IBVP in eqn. (18), is for each maturity, τ_i, measured by the merit-function:

$$\chi^2(\vartheta_i(\mathbf{K})) := \sum_{ij=1}^{m_i} \left(\frac{c(\tau_i, K_{ij}) - \hat{C}(\tau_i, K_{ij}; \vartheta_i(\mathbf{K}))}{w_{ij}} \right)^2, w_{ij} = \frac{\partial c(\tau_i, K_{ij})}{\partial \sigma_{imp}(\tau_i, K_{ij})} \tag{21}$$

Thus, small values of $\chi_i^2(\vartheta_i(\mathbf{K}))$ represents close agreement.

The weights w_{ij} is given by the greek *vega* in the Black-Scholes model. As known, this quantity measures the sensitivity of the call price towards changes in the volatility parameter. Hence, the influence of a measurement error contained in the observed data, is reduced by assigning a relative smaller weight to strike levels with high sensitivity.

The theoretical call prices: $\{\hat{C}(\tau_i, K_j; \vartheta_i(K_j))\}_{j=0,\ldots,m}$, for time-to-maturity τ_i is calculated by one time step in the implicit finite difference method, see eqn. (18)-(20). Hence, by solving a system of linear equations:

$$\mathbf{A}_i \cdot \hat{C}(\tau_i, \mathbf{K}) = \hat{C}(\tau_{i-1}, \mathbf{K}) \tag{22}$$

where $\hat{C}(\tau_0, \mathbf{K})$ is given by the initial condition (19) and $\mathbf{A}_i$ is the tridiagonal matrix given below:

$$\mathbf{A}_i = \begin{bmatrix} 1 & 0 & 0 & \cdots & \cdots & 0 \\ -z_1^i & 1+2z_1^i & -z_1^i & 0 & \cdots & \vdots \\ 0 & -z_2^i & 1+2z_2^i & -z_2^i & \ddots & \vdots \\ \vdots & \ddots & \ddots & \ddots & \ddots & 0 \\ \vdots & \ddots & 0 & -z_{m-1}^i & 1+2z_{m-1}^i & -z_{m-1}^i \\ 0 & \cdots & \cdots & 0 & 0 & 1 \end{bmatrix} \tag{23}$$

where the coefficients z_j^i is given by:

$$z_j^i = \frac{1}{2}\frac{\Delta\tau_i}{\Delta K^2}\vartheta_i(K_j)^2 K^2 \qquad j = 2, \ldots, m-1.$$

The theoretical call price for a specific observed strike K_{ij} is determined from the vector of call prices $\hat{C}(\tau_i, \mathbf{K})$ by linear interpolation.

The flow of the calibration technique is illustrated in figure 7.

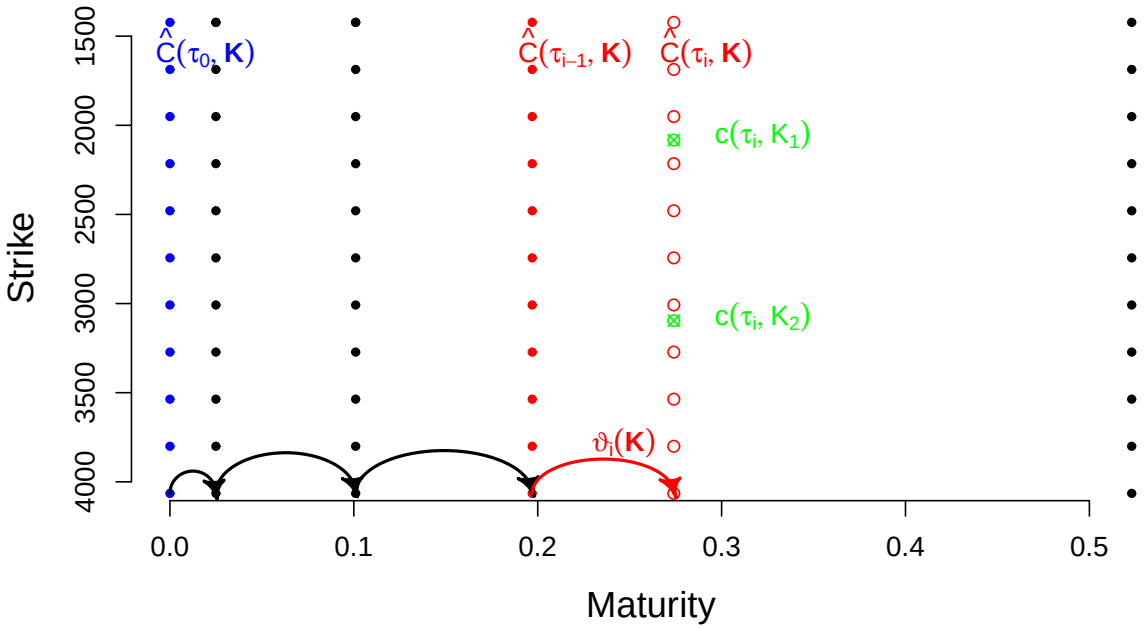

Figure 7: Illustration of a grid containing calibrated call prices for τ_0 up to τ_{i-1}. The call prices for τ_i is fitted by adjusting the parameter $\vartheta_i(K)$ according to the observed data.

5.2.2 Fitting the Proxy's

The minimization problem given in eqn. (21) is solved separately for each of the n observed maturities by the *Levenberg-Marquardt* algorithm given in Press et al. (see 2007, ch. 15.5.2). This is a standard non-linear least-square routine and it works well for problems where a plausible initial guess can be provided.

The obvious initial guess for this optimization procedure, $\vartheta_i^{ini}(\mathbf{K})$, is given by the implied volatilities observed in the market.

For each iteration in the optimization algorithm is a set of theoretical call prices $\hat{C}(\tau_i, \mathbf{K})$ determined by solving the system of equations given in eqn. (22). The structure of the matrix $\mathbf{A}_i$, given in eqn. (23), reveals that this is a simple tridiagonal band-matrix. Hence, this system can be solved in linear time $\mathcal{O}(n)$ using *LU-decomposition*.

Pseudo code:

- For $i = 1, \ldots, n$ do:
  - Calibrate the parameter $\vartheta_i(\mathbf{K})$ - and the corresponding set of call prices $\hat{C}(\tau_i, \mathbf{K})$ - by minimizing the merit-function in eqn. (21) by using the *Levenberg-Marquardt* algorithm.
  - For each of the x iterations, involved in the optimization procedure, the theoretical call prices is determined by solving a system of equations for one time step in the implicit finite difference method.

5.2.3 Deriving the call surface

The theoretical call prices $\hat{C}(\tau_i, \mathbf{K})$ and the piecewise constant volatility proxy's $\vartheta_i^2(\mathbf{K})$ are given for all the observed time-to-maturities: $\{\tau_i\}_{i=1,\ldots,n}$, after the calibration has been carried out as described in the previous section.

The complete surface of calibrated European call prices can then be obtained by interpolating between the observed maturities by using the implicit finite difference solver.

Let initially a new uniform grid with smaller steps for the time dimension be given by:

$$\tau_l = \tau_0 + l\Delta\tau \qquad \text{for } l = 1, \ldots, N.$$

where $\Delta\tau = (\tau_n - \tau_0)/N$ and $N > n$.

Hence, the European call prices for all intermediate time-to-maturities:

$$\tau_l \in (\tau_{i-1}; \tau_i) \qquad i = 1, \ldots, n$$

must then be calculated in order to obtain the (discrete) surface of European call price approximations.

Usually, when using a finite difference method, these prices are derived by iterating forward in time by solving the system below:

$$\left[1 - \frac{1}{2}\Delta\tau\vartheta_i^2(\mathbf{K})\mathbf{K}^2\delta_{KK}\right]\hat{C}(\tau_l, \mathbf{K}) = \hat{C}(\tau_{l-1}, \mathbf{K}) \quad \text{for } \tau_l \in (\tau_{i-1}, \tau_i)$$

for each of the intermediate maturities. This principle - which was also used previously for the observable maturities - is illustrated in figure 8.

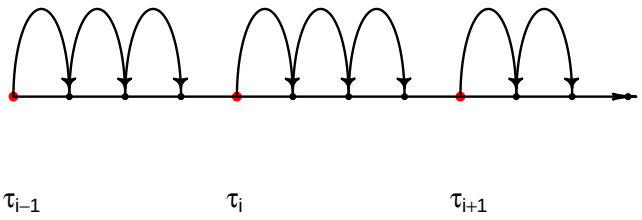

Figure 8: Illustration of the normal procedure for calculating the intermediate call prices using a FDM.

The advantage of this procedure - seen through traditional glasses - is that it converges (under sufficient regulations) when $\Delta K \to 0$ and $\Delta\tau \to 0$. But as the call prices generated by this procedure is arbitrage free regardless of the step size in the underlying grid (see section 6) there is no particular need for this convergence property.

Instead Andreasen and Huge propose to *fill the gaps* between the observed maturities by stepping directly from τ_{i-1} to each of the time points τ in the interval (τ_{i-1}, τ_i). In practice, this is done by solving the equation below:

$$\left[1 - \frac{1}{2}(\tau_l - \tau_{i-1})\vartheta_i^2(K_j)K_j^2\delta_{KK}\right]\hat{C}_{i,j} = \hat{C}_{i-1,j}, \quad \tau_l \in (\tau_{i-1}, \tau_i) \tag{24}$$

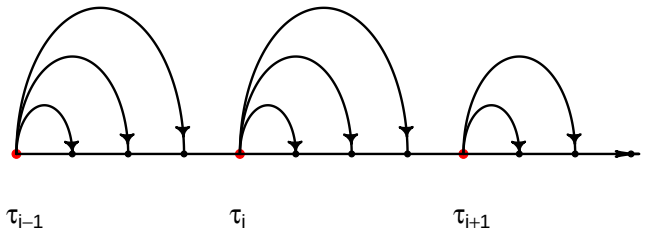

Figure 9: Illustration of the alternative procedure proposed by Andreasen and Huge for calculating the intermediate call prices using a FDM.

This alternative procedure illustrated in figure 9.

Remark that the approximations: $\hat{C}_{l,j}$, will not converge as the number of grid points, N, is increases as a consequence of this construction. This is due to the fact that individual time step $\tau_l - \tau_{i-1}$ will not decrease as the grid gets denser.

The approximation is though still capable of converging towards the semi-discrete approximation: $\tilde{C}(\tau_i, \mathbf{K})$, as the number of grid points m in the strike dimension is increased.

Thus, the semi-discrete version of eqn. (24) is given by:

$$\left[1 - \frac{1}{2}(\tau_l - \tau_{i-1})\vartheta_i^2(K)K^2\frac{\partial^2}{\partial K^2}\right]\tilde{C}(\tau_l, K) = \tilde{C}(\tau_{i-1}, K), \quad \tau_l \in (\tau_{i-1}, \tau_i) \tag{25}$$

Pseudo-code:

- For $l = 1, \ldots, N$ do:
  - Calculate the approximations $\hat{C}_{l,j}$ for all m grid points in the strike dimension by solving eqn. (24).

5.3 Deriving the local volatility surface

The final part of the method is to derive the actual local volatility function $\sigma^2(\tau + t, K)$ from the surface of call prices calibrated by the technique pre-

sented in the previous sections.

As an entire surface of call prices is now available, this parameter can be determined from a finite difference discretsation of the *Dupire formula* given in eqn. (15):

$$\sigma^2(\tau_l + t, K_j) = 2\frac{\frac{1}{\Delta\tau}\left(\hat{C}(\tau_l, K_j) - \hat{C}(\tau_{l-1}, K_j)\right)}{\frac{K_j^2}{\Delta K^2}\left(\hat{C}(\tau_l, K_{j+1}) - 2\hat{C}(\tau_l, K_j) + \hat{C}(\tau_l, K_{j-1})\right)} \tag{26}$$

This discrete surface is well-defined according to the continuous time theory in section 3.1 if the convexity in strike and the slope in maturity of the call prices are strictly positive. Thus, if the given arbitrage conditions presented in section sec:absArb are satisfied with strict inequality.

Pseudo-code:

- For $l = 2, \ldots, N$ do:
  - For $j = 2, \ldots, m-1$ do:
    - Calculate the finite differences $\delta_{KK}\hat{C}_{l,j}$ and $\delta_{\tau}\hat{C}_{l,j}$. Determine the local volatility parameter $\sigma^2(\tau_l + t, K_j)$ from these.

6 Absence of arbitrage

The discrete surface of calibrated approximations to European call price, from which the discrete local volatility surface are extracted, must be arbitrage free in order to secure consistent pricing.

Carr and Madan (2005) establish in their paper: *A note on sufficient conditions for no arbitrage*, sufficient conditions under which a rectangular grid of European option prices is free of *static arbitrage*. The authors define *Static arbitrage* as a costless trading strategy where the position taken in the underlying stock is only allowed to depend on time and the current stock price. This is opposed to the general concept of *arbitrage*, where the trading strategy is allowed to depend on a larger set of information that can be difficult to determine in practice.

The sufficient conditions for absence of arbitrage in the discrete surface of call prices $\{\hat{C}(\tau_l, K_j)\}$[15] is according to Carr and Madan:

- Non-increasing in strike:

$$\delta_K \hat{C}(\tau_l, K_j) = \frac{\hat{C}(\tau_l, K_j) - \hat{C}(\tau_l, K_{j-1})}{\Delta K} \leq 0$$

- Convex in strike:

$$\delta_{KK} \hat{C}(\tau_l, K_{j-1}) = \frac{\hat{C}(\tau_l, K_{j-1}) - 2\hat{C}(\tau_l, K_j) + \hat{C}(\tau_l, K_{j+1})}{\Delta K^2} \geq 0$$

- Non-decreasing in maturity:

$$\delta_\tau \hat{C}(\tau_l, K_j) = \frac{\hat{C}(\tau_l, K_j) - \hat{C}(\tau_{l-1}, K_j)}{\tau_l - \tau_{l-1}} \geq 0$$
$$\overset{\diamond}{\Rightarrow} \frac{\partial \hat{C}}{\partial \tau}(\tau_l, K_j) \geq 0$$

$\diamond$: The two maturities τ_l and τ_{l-1} can by construction of the method be chosen arbitrarily close, see (27).

[15] Remark that τ_l is only notation for a given maturity within the region of observed maturities. It does not have to be generated by an equidistant discretization as in the implementation.

Translated to the semi-discrete surface of call prices $\{\tilde{C}(\tau_l, K)\}$ that is assumed to be continuous in strike, this corresponds to the following conditions:

$$\frac{\partial \tilde{C}}{\partial K}(\tau_l, K) \leq 0, \quad \frac{\partial^2 \tilde{C}}{\partial K^2}(\tau_l, K) \geq 0, \quad \frac{\partial \hat{C}}{\partial \tau}(\tau_l, K) \geq 0$$

for all (τ_l, K) within the semi-discrete grid defined by the observable strikes and maturities.

Remark that if the convexity condition and the maturity condition are satisfied with strict inequality then will the volatility function, derived through either eqn. (26) or eqn. (12), be positive which is required for the local volatility model to be well-defined cf. eqn. (1).

6.1 Semi-discrete argument

In section 5.2.2 it was described how the step size in the spatial domain could be reduced such that the discrete approximation, $\hat{C}(\cdot)$, would converge towards the semi-discrete approximation, $\tilde{C}(\cdot)$.

Thus, the semi-discrete surface of European call prices is assumed to be generated by solving the generalized forward PDDE for $i = 1, \ldots, n$:

$$\left[1 - \frac{1}{2}(\tau - \tau_{i-1})\vartheta_i^2(K)K^2\frac{\partial^2}{\partial K^2}\right]\tilde{C}(\tau, K) = \tilde{C}(\tau_{i-1}, K), \quad \tau \in (\tau_{i-1}, \tau_i] \quad (27)$$

where the notation τ symbolises that the equation holds for any τ on the given interval.

The solution $\tilde{C}(\tau, K)$ to the PDE above can also be written as the integral below:

$$\tilde{C}(\tau, K) = \frac{1}{\tau - \tau_{i-1}}\int_0^\infty \exp\left(\frac{-u}{\tau - \tau_{i-1}}\right) C_\vartheta(u, K)du \quad \tau > \tau_{i-1} \qquad (28)$$

where the function $C_\vartheta(\cdot)$ is the exact solution to the IBVP:

$$0 = -\frac{\partial C_\vartheta}{\partial u}(u, K) + \frac{1}{2}\vartheta_i^2(K)K^2\frac{\partial^2 C_\vartheta}{\partial K^2}(u, K) \quad u > 0 \qquad (29)$$
$$C_\vartheta(0, K) = \tilde{C}(\tau_{i-1}, K)$$

The initial condition is given by the call values for time-to-maturity τ_{i-1}. Assume that these are arbitrage free, as they are either given by the calculations for the previous sub-period, $(\tau_{i-2}, \tau_{i-1}]$, or by the payoff function if $i = 1$.

Proof. Equation (28) can be verified by *Laplace-Carson* transformation or by ordinary *integration by parts*:

$$f(u) = \exp\left(\frac{-u}{\tau - \tau_{i-1}}\right), \quad F(u) = -(\tau - \tau_{i-1}) \exp\left(\frac{-u}{\tau - \tau_{i-1}}\right)$$
$$g(u) = C_\vartheta(u, K), \qquad g'(u) = \frac{\partial C_\vartheta}{\partial u}(u, K)$$

$$\begin{aligned}
\tilde{C}(\tau, K) &= \frac{1}{\tau - \tau_{i-1}} \left([F(u)g(u)]_0^\infty - \int_0^\infty F(u)g'(u)du \right) \\
&= \left[-\exp\left(\frac{-u}{\tau - \tau_{i-1}}\right) C_\vartheta(u, K) \right]_0^\infty + \int_0^\infty \exp\left(\frac{-u}{\tau - \tau_{i-1}}\right) \frac{\partial C_\vartheta}{\partial u}(u, K)du \\
&= \lim_{u\to\infty} \left(-\exp\left(\frac{-u}{\tau - \tau_{i-1}}\right) C_\vartheta(u, K) \right) + \exp(0)\, C_\vartheta(0, K) + \int_0^\infty \cdots du \\
&\overset{(\diamond)}{=} C_\vartheta(0, K) + \int_0^\infty \exp\left(\frac{-u}{\tau - \tau_{i-1}}\right) \frac{\partial C_\vartheta}{\partial u}(u, K)du \\
&\overset{(29)}{=} \tilde{C}(\tau_{i-1}, K) + \int_0^\infty \exp\left(\frac{-u}{\tau - \tau_{i-1}}\right) \frac{1}{2}\vartheta_i^2(K)K^2 \frac{\partial^2 C_\vartheta}{\partial K^2}(u, K)du \\
&= \tilde{C}(\tau_{i-1}, K) + \frac{1}{2}\vartheta_i^2(K)K^2 \frac{\partial^2}{\partial K^2} \int_0^\infty \exp\left(\frac{-u}{\tau - \tau_{i-1}}\right) C_\vartheta(u, K)du \\
&\overset{(28)}{=} \tilde{C}(\tau_{i-1}, K) + \frac{1}{2}\vartheta_i^2(K)K^2 \frac{\partial^2}{\partial K^2}(\tau - \tau_{i-1})\tilde{C}(\tau, K) \\
\Leftrightarrow &\left[1 - \frac{1}{2}(\tau - \tau_{i-1})\vartheta_i^2(K)K^2 \frac{\partial^2}{\partial K^2} \right] \tilde{C}(\tau, K) = \tilde{C}(\tau_{i-1}, K) \quad \tau > \tau_{i-1}
\end{aligned} \tag{30}$$

$(\diamond)$: The first term vanished as $\lim_{u\to\infty} \exp\left(\frac{-u}{\tau-\tau_{i-1}}\right)$ approaches zero exponentially fast.

□

Proposition 2 (Absence of arbitrage; semi-discrete). *The European call prices, $\tilde{C}(\tau, K)$, solving the PDDE in eqn. (27) are arbitrage free for $\tau \in (\tau_{i-1}, \tau_i]$ and $K \in [K_{min}, K_{max}]$ for all $i = 1, \ldots, n$.*

Proof. Proposition 2 is proved by showing that $\tilde{C}(\tau, K)$ satisfies the sufficient arbitrage condtions given in the beginning of this section.

Remark initially that the forward PDE in eqn. (29) is equivalent to the Dupire forward equation in (11) for zero rate and local volatility function, $\sigma^2(\cdot)$, given by:

$$\sigma^2(\tau + t, K) = \vartheta_i^2(K) \qquad \tau \in (\tau_{i-1}, \tau_i].$$

Further remark, that the process $C_\vartheta(u, K)$ is equal to the call price $\tilde{C}(\tau_{i-1}, K)$ at expiry $u = 0$. Thus, $C_\vartheta(u, K)$ is the price process for a call option in the local volatility model and the results from section 3.3 can be used to prove the conditions regarding the derivatives w.r.t. strike.

Non-increasing in strike:
Start by differentiating eqn. (28) once with respect to K:

$$\frac{\partial \tilde{C}}{\partial K}(\tau, K) = \frac{1}{\tau - \tau_{i-1}} \int_0^\infty \exp\left(\frac{-u}{\tau - \tau_{i-1}}\right) \frac{\partial C_\vartheta}{\partial K}(u, K) du \quad \tau \in (\tau_{i-1}, \tau_i]$$

as the first term: $\exp\left(\frac{-u}{\tau - \tau_{i-1}}\right)$, is positive, this implies that:

$$\frac{\partial C_\vartheta}{\partial K}(u, K) \leq 0 \quad \Rightarrow \quad \frac{\partial \tilde{C}}{\partial K}(\tau, K) \leq 0 \tag{31}$$

The first order derivative of $C_\vartheta(u, K)$ is given by eqn. (9):

$$\frac{\partial C_\vartheta}{\partial K}(u, K) = -\int_K^\infty \varphi(0, s; u, S) dS$$

where $\varphi(0, s; u, S)$ is the risk neutral transition density of $S(u) = S$ given $S(0) = s$. Thus, the integral above is positive per definition and it can then be concluded:

$$\frac{\partial C_\vartheta}{\partial K}(u, K) \leq 0 \qquad u \geq 0$$

which in conjunction with eqn. (31) gives the non-increasing call prices $\tilde{C}(\tau, K)$ in the strike direction.

Convexity in strike:
Start by differentiating eqn. (28) twice with respect to K:

$$\frac{\partial^2 \tilde{C}}{\partial K^2}(\tau, K) = \frac{1}{\tau - \tau_{i-1}} \int_0^\infty \exp\left(\frac{-u}{\tau - \tau_{i-1}}\right) \frac{\partial^2 C_\vartheta}{\partial K^2}(u, K) du \quad \tau \in (\tau_{i-1}, \tau_i]$$

this implies that:

$$\frac{\partial^2 C_\vartheta}{\partial K^2}(u,K) \geq 0 \quad \Rightarrow \quad \frac{\partial^2 \tilde{C}}{\partial K^2}(\tau,K) \geq 0 \tag{32}$$

The second order derivative of $C_\vartheta(u,K)$ is given by eqn. (10):

$$\frac{\partial^2 C_\vartheta}{\partial K^2}(u,K) = \varphi(0,s;u,K)$$

where $\varphi(0,s;u,K)$ is the risk neutral transition density of $S(u) = K$ given $S(0) = s$.

Thus, as densities are positive per definition, it can be concluded from this:

$$\frac{\partial^2 C_\vartheta}{\partial K^2}(u,K) = \hat{\varphi}(0,s;u,K) \geq 0$$

which in conjunction with eqn. (32) gives the convexity of the call prices $\tilde{C}(\tau,K)$. This convexity condition will hold with strict inequality if the transition density $\hat{\varphi}(0,s;u,K)$ is assumed to be positive for some $u \geq 0$.

Non-decreasing in maturity:
Instead of differentiating eqn. (28) directly with respect to τ, differentiate the intermediate result (30):

$$\begin{aligned}
\frac{\partial \tilde{C}}{\partial \tau}(\tau,K) &= \frac{\partial}{\partial \tau}\left(\tilde{C}(\tau_{i-1},K) + \int_0^\infty \exp\left(\frac{-u}{\tau-\tau_{i-1}}\right)\frac{1}{2}\vartheta_i^2(K)K^2\frac{\partial^2 C_\vartheta}{\partial K^2}(u,K)du\right) \\
&= \int_0^\infty \frac{\partial}{\partial \tau}\exp\left(\frac{-u}{\tau-\tau_{i-1}}\right)\frac{1}{2}\vartheta_i^2(K)K^2\frac{\partial^2 C_\vartheta}{\partial K^2}(u,K)du \\
&= \int_0^\infty \exp\left(\frac{-u}{\tau-\tau_{i-1}}\right)\frac{u}{(\tau-\tau_{i-1})^2}\frac{1}{2}\vartheta_i^2(K)K^2\frac{\partial^2 C_\vartheta}{\partial K^2}(u,K)du
\end{aligned}$$

The operational sign of the terms in this integral are all known:

- $\frac{u}{(\tau-\tau_{i-1})^2} \geq 0$ as $u \geq 0$ and $\tau > \tau_{i-1}$.
- $\exp\left(\frac{-u}{\tau-\tau_{i-1}}\right) \geq 0$ by definition of the exponential function.
- $\frac{\partial^2 C_\vartheta}{\partial K^2}(u,K) \geq 0$ by the result obtained previously.

The integral in the equation above will therefore be non-negative:

$$\frac{\partial \tilde{C}}{\partial \tau}(\tau, K) \geq 0$$

which gives non-decreasing call prices $\tilde{C}(\tau, K)$ in the time direction. This condition will hold with strict inequality if the convexity condition holds with strict inequality.

The results trivially holds for all $i = 1, \ldots, n$. □

6.2 Discrete argument

The absence of arbitrage in the European call surface, generated by the technique proposed by Andreasen and Huge, is not only arbitrage free in the limit for $\Delta K \to 0$, as will be shown in this section. This implies that the calibration of arbitrage free call prices can be carried out in a coarser grid and thereby reduce the computational cost significantly.

The discrete surface of European call prices is generated by solving the generalized finite difference equation given below for $i = 1, \ldots, n$:

$$\left[1 - \frac{1}{2}(\tau - \tau_{i-1})\vartheta_i^2(K_j)K_j^2\delta_{KK}\right]\hat{C}(\tau, K_j) = \hat{C}(\tau_{i-1}, K_j), \quad \tau \in (\tau_{i-1}, \tau_i] \tag{33}$$

This equation can be written as a system of linear equations for all strikes in the underlying grid:

$$\left[\mathbf{I} - \frac{1}{2}(\tau - \tau_{i-1})\left[\vartheta_i^2(\mathbf{K})\right]\left[\delta_{KK}\right]\right] \cdot \hat{C}(\tau, \mathbf{K}) = \hat{C}(\tau_{i-1}, \mathbf{K}) \quad \tau \in (\tau_{i-1}, \tau_i] \tag{34}$$

where $\mathbf{I}$ is the $m \times m$ identity matrix, $[\vartheta_i^2(\mathbf{K})]$ is a diagonal matrix with $\vartheta_i^2(K_j)K_j^2$ in the diagonal entries and $[\delta_{KK}]$ are the 2^{nd} order difference matrix given by:

$$[\delta_{KK}] = \frac{1}{\Delta K^2}\begin{bmatrix} 0 & 0 & 0 & \cdots & \cdots & 0 \\ 1 & -2 & 1 & 0 & \cdots & \vdots \\ 0 & 1 & -2 & 1 & \ddots & \vdots \\ \vdots & \ddots & \ddots & \ddots & \ddots & 0 \\ \vdots & \ddots & 0 & 1 & -2 & -1 \\ 0 & \cdots & \cdots & 0 & 0 & 0 \end{bmatrix}$$

The 1^{st} and m^{th} row of this matrix is set to zero as the system by assumption has absorbing boundaries $\delta_{KK}\hat{C}(\tau, K_0) = \delta_{KK}\hat{C}(\tau, K_m) = 0$, see eqn. (20).

The terms in the matrix on the RHS of (34) can be collected into a single matrix, $\mathbf{B}_i$, given by:

$$\mathbf{B}_i = \begin{bmatrix} 1 & 0 & 0 & \cdots & \cdots & 0 \\ -z_1^i & 1+2z_1^i & -z_1^i & 0 & \cdots & \vdots \\ 0 & -z_2^i & 1+2z_2^i & -z_2^i & \ddots & \vdots \\ \vdots & \ddots & \ddots & \ddots & \ddots & 0 \\ \vdots & \ddots & 0 & -z_{m-1}^i & 1+2z_{m-1}^i & -z_{m-1}^i \\ 0 & \cdots & \cdots & 0 & 0 & 1 \end{bmatrix}$$

where the coefficients z_j^i is given by:

$$z_j^i = \frac{1}{2}\frac{\tau - \tau_{i-1}}{\Delta K^2}\vartheta_i(K_j)^2 K_j^2 \quad \tau \in (\tau_{i-1}, \tau_i],\ j = 2, \ldots, m-1.$$

Definition 1 (Z-matrix[16]). *The class of Z-matrices are those matrices whose off-diagonal entries are less than or equal to zero. That is, a Z-matrix satisfies:*

$$Z = \{z_{ij}\} \qquad z_{ij} \leq 0 \quad \forall\ i \neq j.$$

The off diagonal entries of the matrix $\mathbf{B}_i$ are all non-positive as $z_j^i \geq 0$. Thus, according to definition 1 $\mathbf{B}_i$ is a Z-matrix.

Definition 2 (M-matrix[17]). *The Z-matrix A is a M-matrix if it satisfies any one of the following two conditions:*

- *A is non-singular and the inverse of A is non-negative.*
- *The diagonal entries of A are positive and AD is strictly diagonally dominant for some positive diagonal matrix D .*

The matrix $\mathbf{B}_i = [b_{kl}^i]$ is strictly diagonal dominant as the following equation is satisfied:

$$|b_{kk}^i| > \sum_{l \neq k} |b_{kl}^i| \quad \forall i = 1, \ldots . n.$$

[16] See Wikipedia: *Z-matrix (mathematics).*
[17] See planetmath.org: *M-matrix*, item *14* and item *6* on the list.

Definition 2 then gives that $\mathbf{B}_i$ is a M-matrix and that the inverse is non-negative:

$$\mathbf{B}_i^{-1} \geq 0 \tag{35}$$

Furthermore, it is easily seen that the rows of this matrix sum to one:

$$\mathbf{B}_i I = I \quad \Leftrightarrow \quad \mathbf{B}_i^{-1} I = I.$$

where I is a m-dimensional vector of 1's.

Thus, as Jesper Andreasen notes in part 2 of his slides from 2011, this means that the rows of matrix $\mathbf{B}_i^{-1}$ can be interpreted as the transition probabilities of going from state K_k at time-to-maturity τ to state K_l at time-to-maturity τ_{i-1}. Thus, each of the European call prices: $\hat{C}(\tau, K_k)$, is given by the expected *payoff* at the end of the sub-period:

$$\hat{C}(\tau, K_k) = \sum_{l=1}^{m} b_{kl}^i \hat{C}(\tau_{i-1}, K_l)$$

Recall that the arbitrage free price of an option is equal to the expected payoff under the risk-neutral measure. Thus, if the prices: $\hat{C}(\tau_{i-1}, \mathbf{K})$, where arbitrage free and if the *transition probabilities* where risk-neutral, then would the call prices: $\hat{C}(\tau, \mathbf{K})$, be arbitrage free. That this is in fact the case is shown below.

Proposition 3 (Absence of arbitrage; discrete)**.** *The European call prices, $\hat{C}(\tau, K_j)$, solving the finite difference equation (33) are arbitrage free for all $\tau \in (\tau_{i-1}, \tau_i]$ and $j = 0, \ldots, m$ for all $i = 1, \ldots, n$.*

Proof. Proposition 3 is proved by showing that $\tilde{C}(\tau, K)$ satisfies the sufficient arbitrage conditions given in the beginning of this section.

Convexity in strike:
Differentiate the discrete system of equation given in (34) twice with respect to the strike by using the difference operator $[\delta_{KK}]$ defined above:

$$\begin{aligned}
&[\delta_{KK}] \left[\mathbf{I} - \frac{1}{2}(\tau - \tau_{i-1}) \left[\vartheta_i^2(\mathbf{K}) \right] [\delta_{KK}] \right] \hat{C}(\tau, \mathbf{K}) = [\delta_{KK}] \hat{C}(\tau_{i-1}, \mathbf{K}) \\
\Leftrightarrow &\left[\mathbf{I} - \frac{1}{2}(\tau - \tau_{i-1}) [\delta_{KK}] \left[\vartheta_i^2(\mathbf{K}) \right] \right] [\delta_{KK}] \hat{C}(\tau, \mathbf{K}) = [\delta_{KK}] \hat{C}(\tau_{i-1}, \mathbf{K}) \\
\Leftrightarrow &[\delta_{KK}] \hat{C}(\tau, \mathbf{K}) = \left[\mathbf{I} - \frac{1}{2}(\tau - \tau_{i-1}) [\delta_{KK}] \left[\vartheta_i^2(\mathbf{K}) \right] \right]^{-1} [\delta_{KK}] \hat{C}(\tau_{i-1}, \mathbf{K})
\end{aligned} \tag{36}$$

Define a matrix $\mathbf{D}_i$ by:

$$\mathbf{D}_i = \left(\mathbf{I} - \frac{1}{2}(\tau - \tau_{i-1}) \left[\delta_{KK}\right] \left[\vartheta_i^2(\mathbf{K})\right] \right)$$

and remark that:

$$\left[\vartheta_i^2(\mathbf{K})\right] \left[\delta_{KK}\right] = \left[\vartheta_i^2(\mathbf{K})\right]^* \left[\delta_{KK}\right]^*, \quad \left[\delta_{KK}\right] \left[\vartheta_i^2(\mathbf{K})\right] = \left[\delta_{KK}\right]^* \left[\vartheta_i^2(\mathbf{K})\right]^*$$

for the symmetric matrix $\left[\vartheta_i^2(\mathbf{K})\right]^*$ equal to $\left[\vartheta_i^2(\mathbf{K})\right]$ with the first and last row set to zero, and the symmetric matrix $\left[\delta_{KK}\right]^*$ given by:

$$\left[\delta_{KK}\right]^* = \frac{1}{\Delta K^2} \begin{bmatrix} -2 & 1 & 0 & \cdots & \cdots & 0 \\ 1 & -2 & 1 & 0 & \cdots & \vdots \\ 0 & 1 & -2 & 1 & \ddots & \vdots \\ \vdots & \ddots & \ddots & \ddots & \ddots & 0 \\ \vdots & \ddots & 0 & 1 & -2 & 1 \\ 0 & \cdots & \cdots & 0 & 1 & -2 \end{bmatrix}$$

Thus:

$$\begin{aligned} \left(\left[\vartheta_i^2(\mathbf{K})\right] \left[\delta_{KK}\right]\right)^T &= \left(\left[\vartheta_i^2(\mathbf{K})\right]^* \left[\delta_{KK}\right]^*\right)^T = \left(\left[\delta_{KK}\right]^*\right)^T \left(\left[\vartheta_i^2(\mathbf{K})\right]^*\right)^T \\ &= \left[\delta_{KK}\right]^* \left[\vartheta_i^2(\mathbf{K})\right]^* = \left[\delta_{KK}\right] \left[\vartheta_i^2(\mathbf{K})\right] \end{aligned}$$

which gives the relation:

$$\left(\mathbf{B}_i\right)^T = \mathbf{D}_i.$$

and according to eqn. (35):

$$\mathbf{D}_i^{-1} = \left(\mathbf{B}_i^T\right)^{-1} = \left(\mathbf{B}_i^{-1}\right)^T \geq 0.$$

If the call prices with maturity τ_{i-1} is arbitrage free, then they will be convex in strike:

$$\left[\delta_{KK}\right] \hat{C}(\tau_{i-1}, \mathbf{K}) \geq 0.$$

which combined with eqn. (36) gives the convexity in strike for the call options with maturity $\tau \in (\tau_{i-1}, \tau_i]$:

$$\left[\delta_{KK}\right] \hat{C}(\tau, \mathbf{K}) = \mathbf{D}_i^{-1} \left[\delta_{KK}\right] \hat{C}(\tau_{i-1}, \mathbf{K}) \geq 0.$$

Non-increasing in strike:

Let the first order one-sided difference matrix $[\delta_K]$ be given by:

$$[\delta_K] = \frac{1}{\Delta K} \begin{bmatrix} 1 & -1 & 0 & \cdots & \cdots & 0 \\ 0 & 1 & -1 & 0 & \cdots & \vdots \\ 0 & 0 & 1 & -1 & \ddots & \vdots \\ \vdots & \ddots & \ddots & \ddots & \ddots & 0 \\ \vdots & \ddots & 0 & 0 & 1 & -1 \\ 0 & \cdots & \cdots & 0 & 0 & 1 \end{bmatrix}$$

Remark that this matrix has positive entries in the top and bottom row as the matrix needs to be invertible in the following. Hence, the differences at the boundaries needs to be considered explicitly in the derivations.

Use the difference matrix above to differentiate the system given in eqn. (34) once with respect to the strike:

$$\begin{aligned} & [\delta_K] \left[\mathbf{I} - \frac{1}{2}(\tau - \tau_{i-1}) \left[\vartheta_i^2(\mathbf{K}) \right] [\delta_{KK}] \right] \hat{C}(\tau, \mathbf{K}) = [\delta_K] \hat{C}(\tau_{i-1}, \mathbf{K}) \\ \Leftrightarrow & \left[[\delta_K] - \frac{1}{2}(\tau - \tau_{i-1}) [\delta_K] \left[\vartheta_i^2(\mathbf{K}) \right] [\delta_{KK}] \right] \hat{C}(\tau, \mathbf{K}) = [\delta_K] \hat{C}(\tau_{i-1}, \mathbf{K}) \\ \Leftrightarrow & \left[\mathbf{I} - \frac{1}{2}(\tau - \tau_{i-1}) [\delta_K] \left[\vartheta_i^2(\mathbf{K}) \right] [\delta_{KK}] [\delta_K]^{-1} \right] [\delta_K] \hat{C}(\tau, \mathbf{K}) = [\delta_K] \hat{C}(\tau_{i-1}, \mathbf{K}) \\ \Leftrightarrow & [\delta_K] \hat{C}(\tau, \mathbf{K}) = \left[\mathbf{I} - \frac{1}{2}(\tau - \tau_{i-1}) [\delta_K] \left[\vartheta_i^2(\mathbf{K}) \right] [\delta_{KK}] [\delta_K]^{-1} \right]^{-1} [\delta_K] \hat{C}(\tau_{i-1}, \mathbf{K}) \end{aligned} \tag{37}$$

It can be shown[18] that the inverse of the difference matrix is given by:

$$[\delta_K]^{-1} = \Delta K \begin{bmatrix} 1 & 1 & 1 & \cdots & \cdots & 1 \\ 0 & 1 & 1 & 1 & \cdots & 1 \\ 0 & 0 & 1 & 1 & \ddots & \vdots \\ \vdots & \ddots & \ddots & \ddots & \ddots & 1 \\ \vdots & \ddots & 0 & 0 & 1 & 1 \\ 0 & \cdots & \cdots & 0 & 0 & 1 \end{bmatrix}$$

Thus, the matrix $[\delta_K] \left[\vartheta_i^2(\mathbf{K}) \right] [\delta_{KK}] [\delta_K]^{-1}$ can be written as:

[18] Either by gaussian elimination or by using a software program such as maple/matlab/R.

$$
\begin{aligned}
[\delta_K] \cdot \frac{1}{\Delta K^2}
&\begin{bmatrix}
0 & 0 & \cdots & 0 \\
\vartheta_i(K_1)^2K_1^2 & -2\vartheta_i(K_1)^2K_1^2 & \vartheta_i(K_1)^2K_1^2 & 0 \\
0 & \vartheta_i(K_2)^2K_2^2 & -2\vartheta_i(K_2)^2K_2^2 & \vartheta_i(K_2)^2K_2^2 \\
\vdots & \ddots & \ddots & \vdots \\
\ddots & 0 & \vartheta_i(K_{m-1})^2K_{m-1}^2 & -2\vartheta_i(K_{m-1})^2K_{m-1}^2 \\
0 & \cdots & 0 & 0
\end{bmatrix} \cdot [\delta_K]^{-1} \\
&= [\delta_K] \cdot \frac{1}{\Delta K}
\begin{bmatrix}
0 & 0 & \cdots & 0 \\
\vartheta_i(K_1)^2K_1^2 & -\vartheta_i(K_1)K_1^2 & 0 & \cdots \\
0 & \vartheta_i(K_2)^2K_2^2 & -\vartheta_i(K_2)^2K_2^2 & 0 \\
\vdots & \ddots & \ddots & \vdots \\
\ddots & 0 & \vartheta_i(K_{m-1})^2K_{m-1}^2 & -\vartheta_i(K_{m-1})^2K_{m-1}^2 \\
0 & \cdots & 0 & 0
\end{bmatrix} \\
&= \frac{1}{\Delta K^2}
\begin{bmatrix}
-\vartheta_i(K_1)^2K_1^2 & \vartheta_i(K_1)^2K_1^2 & \cdots & 0 \\
\vartheta_i(K_1)^2K_1^2 & -(\vartheta_i(K_1)^2K_1^2 + \vartheta_i(K_2)^2K_2^2) & \vartheta_i(K_2)^2K_2^2 & \cdots \\
0 & \vartheta_i(K_2)^2K_2^2 & -(\vartheta_i(K_2)^2K_2^2 + \vartheta_i(K_3)^2K_3^2) & \vdots \\
\vdots & \ddots & \ddots & 0 \\
\ddots & 0 & \vartheta_i(K_{m-1})^2K_{m-1}^2 & -(\vartheta_i(K_{m-1})^2K_{m-1}^2 + \vartheta_i(K_m)^2K_m^2) \\
0 & \cdots & \cdots & 0
\end{bmatrix}
\begin{bmatrix}
0 \\
\cdots \\
0 \\
\vdots \\
0 \\
\vartheta_i(K_m)^2K_m^2
\end{bmatrix}
\end{aligned}
$$

The top row in the matrix above stems from the derivatives at the boundary and this row is therefore be replaced by a row of zeros. It can then be seen that that the matrix:

$$\left[\mathbf{I} - \frac{1}{2}(\tau - \tau_{i-1})\left[\delta_K\right]\left[\vartheta_i^2(\mathbf{K})\right]\left[\delta_{KK}\right]\left[\delta_K\right]^{-1}\right]$$

has negative entries off the diagonal and positive entries on the diagonal. Thus, according to definition 1 this matrix is a Z-matrix. As it furthermore is strictly diagonal dominant, definition 2 gives that it is a M-matrix and that its inverse is non-negative.

If the call prices with maturity τ_{i-1} is arbitrage free, then they will be non-increasing in strike:

$$\left[\delta_K\right]\hat{C}(\tau_{i-1}, \mathbf{K}) \leq 0.$$

which combined with eqn. (37) gives the non-increase in strike for the call options with maturity $\tau \in (\tau_{i-1}, \tau_i]$:

$$\left[\delta_K\right]\hat{C}(\tau, \mathbf{K}) = \left[\mathbf{I} - \frac{1}{2}(\tau - \tau_{i-1})\left[\delta_K\right]\left[\vartheta_i^2(\mathbf{K})\right]\left[\delta_{KK}\right]\left[\delta_K\right]^{-1}\right]^{-1}\left[\delta_K\right]\hat{C}(\tau_{i-1}, \mathbf{K}) \leq 0$$

Non-decreasing in maturity:

Let $\delta\tau$ be the usual difference operator:

$$\delta\tau f(\tau, y) = \frac{f(\tau, y) - f(\tau - \Delta\tau, y)}{\Delta\tau}$$

Use this to differentiate each component of the system given in eqn. (34) with respect to the time-to-maturity:

$$\begin{aligned}
&\left[\delta_\tau\right]\left[\mathbf{I} - \frac{1}{2}(\tau - \tau_{i-1})\left[\vartheta_i^2(\mathbf{K})\right]\left[\delta_{KK}\right]\right]\hat{C}(\tau, \mathbf{K}) = \left[\delta_\tau\right]\hat{C}(\tau_{i-1}, \mathbf{K}) \\
\Leftrightarrow &\left[\left[\delta_\tau\right]\mathbf{I} - \frac{1}{2}\left[\delta_\tau\right](\tau - \tau_{i-1})\left[\vartheta_i^2(\mathbf{K})\right]\left[\delta_{KK}\right]\right]\hat{C}(\tau, \mathbf{K}) = \left[\delta_\tau\right]\hat{C}(\tau_{i-1}, \mathbf{K}) \\
\Leftrightarrow &\left[\left[\delta_\tau\right]\mathbf{I} - \frac{1}{2}\left[\delta_\tau\right]\left[\vartheta_i^2(\mathbf{K})\right]\left[\delta_{KK}\right]\right]\hat{C}(\tau, \mathbf{K}) = \left[\delta_\tau\right]\hat{C}(\tau_{i-1}, \mathbf{K}) \\
\overset{\diamond}{\Leftrightarrow} &\frac{\partial\hat{C}}{\partial\tau}(\tau, \mathbf{K}) = \frac{\partial\hat{C}}{\partial\tau}(\tau_{i-1}, \mathbf{K}) + \frac{1}{2}\left[\vartheta_i^2(\mathbf{K})\right]\left[\delta_{KK}\right]\hat{C}(\tau, \mathbf{K}) \qquad (38)
\end{aligned}$$

◇ Since the call price per construction can be calculated for arbitrary $\tau \in (\tau_{i-1}, \tau_i]$, let $\Delta\tau \to 0$.

If the call prices with maturity τ_{i-1} is arbitrage free, then they will be non-decreasing in time-to-maturity:

$$\frac{\partial}{\partial\tau}\hat{C}(\tau_{i-1}, \mathbf{K}) \geq 0.$$

which combined with eqn. (38) and the convexity in strike gives the non-decrease in time-to-maturity for the call options with maturity $\tau \in (\tau_{i-1}, \tau_i]$:

$$\frac{\partial\hat{C}}{\partial\tau}(\tau, \mathbf{K}) = \frac{\partial\hat{C}}{\partial\tau}(\tau_{i-1}, \mathbf{K}) + \frac{1}{2}\left[\vartheta_i^2(\mathbf{K})\right][\delta_{KK}]\,\hat{C}(\tau, \mathbf{K}) \geq 0$$

Proposition 3 can now be proved by induction:

- For $i = 1$ are the call prices: $\hat{C}(\tau_{i-1}, \mathbf{K})$ given by the initial condition and is thus arbitrage free. Then are the call prices: $\hat{C}(\tau, \mathbf{K})$ for $\tau \in (\tau_0, \tau_1]$ arbitrage free by the three results given above.
- For $i = 2, \ldots, n$ assume that call prices: $\hat{C}(\tau_{i-1}, \mathbf{K})$ are arbitrage free. Then are the call prices: $\hat{C}(\tau, \mathbf{K})$ for $\tau \in (\tau_{i-1}, \tau_i]$ arbitrage free by the three results above.

□

Remark that if $[\delta_{KK}]\hat{C}(\tau_{i-1}, \mathbf{K})$ is strictly positive, then will both of the conditions for convexity in strike and slope in maturity be satisfied for a strict inequality - because of the structure of the matrix $\mathbf{B}_i$.

This condition will not be satisfied for all strike levels when $i = 1$. That is why there in practice often are seen some imperfections for small values of τ in the local volatility surface derived by this method.

7 Calibration in practice

The data used for the numerical examinations is borrowed from the article by Andreasen and Huge (2011). The data is quoted in implied Black Scholes volatilities for European-style options written on the SX5E index and consists of 155 quotes dispersed over 12 maturities and 26 strike levels. The data are provided in appendix A in table 8 and in terms of call prices in table 9.

The strike levels in this section are given as percentage of the spot level as in the original article. This eases the comparison between the results from the article and some of the results presented here.

The calibration method described in the section 5 is implemented in 'C++' and ran on a laptop with Intel(R) Core(TM)2 Duo processor P8600, 2.40GHz.

7.1 Base Case

Initially the constants: K_{min}, K_{max}, ΔK and Tol, used for the calibration are determined. The constant Tol is used in the Levenberg-Marquardt algorithm in connection with the *stopping mechanism* for the iterations. The closer to zero the value of Tol is, the more restrictive is the condition for terminating the iteration, see the enclosed code for further details on the implementation.

Table 1 displays the values: χ_i^2 - of the merit function given in eqn. (21) for different choices of constants, the CPU time - given in seconds, the average χ^2 and the average number of iterations.

The boundaries for the first column is given by the smallest and biggest observed strike $-/+500$, respectively. The values of χ_i^2 reveals, that the fit for the smallest and a range of the largest observed maturities is poor compared to the maturities in the middle of the grid. A closer investigation of the calibrated proxy levels a_{ij} suggests, that this could be due to the boundary values, which seems too small. Thus, the grid is widened for the results in column 2 and 3. The conclusion from this is, that boundaries:

$$K_{min} = \min_{ij} K_{ij} - 1000 \qquad K_{max} = \max_{ij} K_{ij} + 1000$$

are suitable.

The next constant to be changed - in column 4 - is the tolerance level: Tol, which is decreased to $1e-10$. On one hand this change significantly improves the minimization procedure, and gives a better fit for all the observed

Sec's	3.65	3.69	7.02	12.96	195.3	326.26	2.05
Tol	1.00E-003	1.00E-003	1.00E-003	1.00E-010	1.00E-010	1.00E-010	1.00E-010
ΔK	1	1	1	1	0.1	0.05	10
K_{min}	922	422	0	422	422	422	422
K_{max}	4564	5064	5564	5064	5064	5064	5064
τ_i	χ_i^2	χ_i^2	χ_i^2	χ_i^2	χ_i^2	χ_i^2	
0.025	1.41E-04	3.68E-08	1.41E-04	1.47E-24	1.26E-23	4.53E-21	1.59E-27
0.101	4.81E-26	2.26E-28	6.02E-27	4.06E-28	4.92E-24	4.21E-24	3.82E-29
0.197	6.25E-24	6.05E-24	6.45E-24	1.32E-28	6.06E-25	1.95E-22	3.29E-31
0.274	1.08E-25	1.32E-25	5.11E-26	2.63E-26	7.99E-23	9.73E-23	2.46E-29
0.523	4.50E-26	6.06E-26	6.66E-26	7.79E-27	2.82E-24	1.21E-23	1.31E-29
0.772	2.84E-27	4.84E-26	5.41E-26	5.32E-27	3.77E-23	1.18E-23	6.41E-30
1.769	1.31E-20	1.42E-20	1.99E-20	7.49E-27	1.08E-23	3.73E-23	8.81E-29
2.267	7.51E-27	4.42E-27	1.43E-26	9.90E-28	1.05E-23	2.41E-23	1.16E-30
2.784	9.67E-14	1.90E-25	1.57E-25	2.37E-26	2.33E-23	5.59E-23	4.75E-29
3.781	1.94E-04	2.34E-06	2.45E-06	3.11E-08	3.30E-08	4.30E-08	1.12E-08
4.778	5.72E-04	1.18E-04	9.05E-05	3.78E-06	3.76E-06	3.74E-06	3.91E-06
5.774	4.54E-04	3.73E-25	5.00E-26	3.58E-26	2.80E-23	2.48E-24	1.00E-29
Avg χ_i^2	1.13E-04	1.00E-05	1.95E-05	3.18E-07	3.16E-07	3.16E-07	3.26E-07
Avg # iter	4.830	5.083	4.667	22.833	32.667	25.250	29.75

Table 1: Values of χ_i^2 for different choices of constants. The results is based on the data in table 8 and the algorithm described in section 5.

maturities. But on the other hand the computational cost is increased from 3.69 seconds to 12.96.

This increase in computational time is caused by the additional number of iterations on average which increases from 5.1 to 22.8. The calculations reveals that this increase is not uniformly distributed over the maturities, but is concentrated on $2-3$ maturities. This problematic is further discussed below.

The remaining columns contains data for different step sizes in the spatial domain of the underlying grid. The computational cost explodes as the step size is reduced, but the fit does not seem to be improved by this additional investment. On the contrary are the χ_i^2 values increased as the step size decreases, and decreased when the step size is increased, with a couple of exceptions for the critical areas. But the calibrated volatility levels seems to reach a steady level for $\Delta K \leq 1$, and $\Delta K = 1$ is therefore chosen for the remaining calculations.

A test in the Black-Scholes model of the pure FDM part of the implementation shows, that the system converges fast as $\Delta K \to 0$. The *dis-convergence* displayed above is thus likely to be caused by the optimization procedure and any difficulties it might experience for small step sizes. Generally the implementation of the optimization procedure seems to lack robustness.

As previously mentioned, the number of iterations is not uniformly distributed over the range of observed maturities. They are concentrated on the maturities: 0.025, 3.781 and 4.778, as can be seen in table 3. That there are problems in the optimization procedure becomes evident when looking at the volatility levels $\{a_{ij}\}$ in table 2.

	0.025	0.101	0.197	0.274	0.523	0.772	1.769	2.267	2.784	3.781	4.778	5.774
51.31									59.06	45.76		
58.64									39.75	43.20	24.25	
65.97									42.76	31.17	*808096713*	
73.3									38.78	47.91	102.3	
76.97				55.36	40.47	41.06	39					
80.63				34.97	35.44	38.31	31.62	35.19	28.85	30.33	27.40	47.82
84.3				37.5	34.62	29.31	43.81					
86.13	21.02											
87.96	24.23	30.84	34.45	31.42	32.24	35.89	24.3	27.24	33.52	31.38	32.65	34.62
89.79	21.63	30.04	32.45									
91.63	21.89	28.57	28.74	29.31	29.84	26.42	34.84					
93.46	21.38	30.31	27.56									
95.29	22.27	28.7	24.96	26.22	26.89	29.86	24.76	26.13	29.12	21.00	32.93	30.11
97.12	24.40	26.95	25.89									
98.96	30.41	27	23.16	24.45	24.88	23.27	24.3					
100.79	27.43	23.75	22.06									
102.62	18.78	22.22	20.82	20.88	22.14	22.70	33.49	21.17	22.69	*1.407e+09*	20.18	27.93
104.45	13.82	19.49	19.3									
106.29	11.31	17.38	19.42	18.86	20.03	19.80	21.04					
108.12	9.878	14.56	18.45									
109.95	8.123	14.82	15.38	17.97	18.15	18.77	23.64	21.24	25.34	18.00	27.09	26.53
111.78	*-4.917*	11.31	15.44									
113.62				15.19	16.19	17.51	19.17					
117.28				16.95	14.3	15.77	20.09	17.40	18.53	28.05	17.51	25.24
120.95				13.52	13.29	16.21	18.57					
124.61				14.08	12.63	13.31	15.19		23.06	15.14	25.7	22.52
131.94									17.73	25.82	19.17	21.63
139.27									25.6	16.25	17.65	28.3
146.6									10.81	22.22	26.06	

Table 2: Volatility levels: a_{ij}, for the data in table 8 with constants: ΔK =1, $K_{min} = 422$,$K_{min} = 5064$ and $tol = 1e - 10$.

Remark the values around the points (τ, K): $(0.025, 111.78)$, $(3.781, 102.62)$ and $(4.778, 58.64)$, looks rather peculiar. The observed data shows that a rough estimate for δ_{KK} is less than -0.3 in these areas. This could suggest that there are some kind of arbitrage or errors[19] in the observed data.

These odd values result in large areas of the calibrated call surface where $\delta_{KK} = 0$ which in turn result in useless local volatility approximations.

As Levenberg-Marquardt algorithm is quite sensitive towards the initial guess, one way for trying to correct these odd volatility levels, is to change the initial guess. A change in the observed implied volatility levels - which are provided as initial guesses - for the given observations or observations in the neighbourhood does adjust the levels, but not enough.

Another approach is to reduce the number of volatility levels for the maturities containing the problematic observations. This gives the optimization

[19]This could be due to the bid-ask spread for the quoted option prices.

procedure an additional degree of freedom for fitting the observations. Replacing the two b_{ij}'s between strike 95.29 & 100.79 and 100.79 & 109.95 with a single b_{ij} in the middle, solves the issue for $\tau = 3.781$. But for $\tau = 4.778$ this only moves the problem to the volatility level around strike 146.6 and for $\tau = 0.025$ it does seem to have any effect at all.

The last attempt is to remove the *bad* observations. For maturity $\tau = 0.025$ the problem with very small values covers a whole area, and removing one of the observations does not correct the other values. While removing observations $(3.781, 95.29)$ and $(4.778, 58.64)$ completely eliminates the problem areas for these maturities. Thus, these are removed from the data and the odd values for $\tau = 0.025$ are kept in mind when examining the results below.

The impact of removing problematic data on the computations can be seen in table 3 and the new volatility levels $\{a_{ij}\}$ are given in appendix A in table 10.

	Org		Clean	
Sec's	10.59		3.56	
τ_i	χ_i^2	# iter	χ_i^2	# iter
0.025	1.47E-024	17	1.47E-024	17
0.101	4.06E-028	7	4.06E-028	7
0.197	1.32E-028	7	1.32E-028	7
0.274	2.63E-026	7	2.63E-026	7
0.523	7.79E-027	7	7.79E-027	7
0.772	5.32E-027	7	5.32E-027	7
1.769	7.49E-027	8	7.49E-027	8
2.267	9.9E-028	6	9.9E-028	6
2.784	2.37E-026	7	2.37E-026	7
3.781	3.11E-08	51	1.42E-026	8
4.778	3.78E-06	203	3.32E-027	7
5.774	3.58E-26	7	4.81E-026	7

Table 3: The number of iterations, the χ_i^2 values and the run-time in seconds for the data with and without observations: $(3.718, 95.29)$ and $(4.778, 58.64)$. The constants are set to: ΔK =1, $K_{min} = 422$,$K_{min} = 5064$ and $tol = 1e{-}10$.

Andreasen and Huge (2011) measures the *calibration accuracy* as the difference between the implied volatility observed in the market and the implied volatilities derived from the option prices generated by the method. The *calibration accuracy* for the *cleansed* data is satisfactory for the constants chosen earlier and can be seen in table 4.
The interpolation between the observed maturities is carried out in a uniform grid consisting of 100 grid points corresponding to step size: $\Delta\tau = 0.06$.

	0.025	0.101	0.197	0.274	0.523	0.772	1.769	2.267	2.784	3.781	4.778	5.774
51.31									0.004	0.003		
58.64									0.002	0.005		
65.97									0.004	0.004	0.003	
73.3									0.002	6e-04	8e-04	
76.97				-0.006	0.002	0.004	0.003					
80.63				6e-04	0.007	0.005	0.003	-0.003	-0.001	-0.002	-0.002	-0.002
84.3				0.003	0.005	0.003	-0.001					
86.13	-0.04											
87.96	-0.03	5e-04	0.004	0.005	0.003	-2e-04	-0.006	-0.004	-0.003	-0.002	-0.001	-8e-04
89.79	-0.02	6e-05	0.004									
91.63	-0.01	0.004	0.007	0.002	-0.002	-0.004	-0.003					
93.46	-0.005	0.005	0.002									
95.29	4e-04	0.001	-0.002	-0.004	-0.005	-0.004	4e-04	-0.001	-0.001		-0.001	-0.002
97.12	0.006	-0.004	-0.005									
98.96	-0.007	-0.003	7e-04	0.002	-2e-05	0.001	0.003					
100.79	-0.004	-2e-04	0.003									
102.62	0.005	-0.003	-0.004	-0.004	-0.002	-6e-04	-0.002	3e-05	-1e-04	-0.001	-0.001	-0.002
104.45	-2e-04	0.002	-0.002									
106.29	-0.008	0.005	0.002	6e-04	-0.003	-0.004	-0.005					
108.12	-0.02	4e-04	0.003									
109.95	-0.02	-0.003	0.001	0.002	0.002	-4e-04	-0.002	-0.003	-0.003	-0.003	-0.001	-0.001
111.78	-0.02	-0.008	-1e-04									
113.62				3e-04	0.002	0.002	-0.001					
117.28				-0.006	0.002	0.001	0.002	-0.003	-0.002	-0.002	-0.002	-0.002
120.95				-0.009	-0.002	0.002	1e-04					
124.61				-0.02	-0.007	-0.002	0.003		0.002	2e-04	-3e-05	-0.002
131.94									0.005	0.002	0.002	-0.001
139.27									0.003	0.003	0.005	-0.001
146.6									0.003	0.002	0.003	

Table 4: Calibration accuracy for the data without observations $(3.718, 95.29)$ and $(4.778, 58.64)$ for constants: ΔK =1, K_{min} = 422,K_{min} = 5064 and $Tol = 1e - 10$.

The calibrated local volatility surface within an area formed by the observed strikes and maturities is given in figure 10. This surface is not smooth in the traditional sense, but the important thing is, that it does not contain spikes or infinite values.

Though there are some irregularities for the first or the first two maturity levels as expected, see the discussion in section 6 at the end of the discrete case.

The local volatilities can be expanded outside this area by using a suitable extrapolation technique directly on the fitted local volatilities.

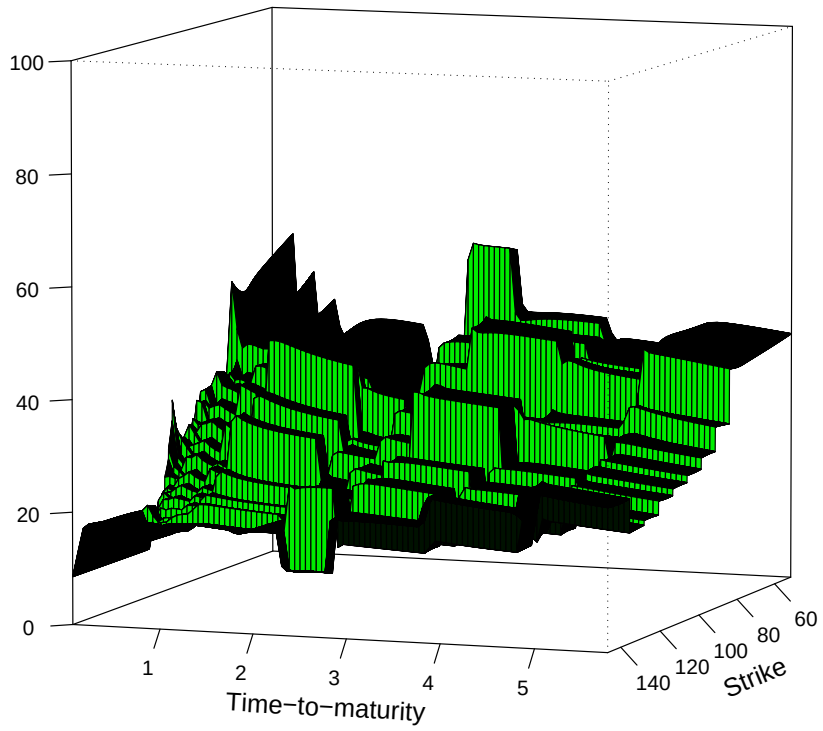

Figure 10: The local volatility surface calibrated to the data in table 8 without observations $(3.718, 95.29)$ and $(4.778, 58.64)$ for constants: ΔK =1, $K_{min} = 422$,$K_{min} = 5064$, $\Delta\tau = 0.06$ and $Tol = 1e - 10$.

7.2 Speed it up

The computational cost for executing the calibration process, can be significantly reduced by a coordinate transformation. The possible gains by a coordinate transformation, according to Tavella and Randall (2000), include:

- better performance.
- fewer grid points for a given accuracy or better accuracy for a given level of computational work.

Note however the simple time coordinate transformation performed in section 5.1.1, where only implemented to ease the notation.

One of the simplest space coordinate transformations is the time-independent one-dimensional logarithmic transform:

$$\xi = \ln(K) \quad \text{or} \quad K = \exp(\xi).$$

This transformation concentrates the spatial grid on a much smaller scale as seen in figure 11(a). Thus, the calibration can be carried out in a much smaller grid while retaining a given accuracy level and thereby reduce the computational cost significantly.

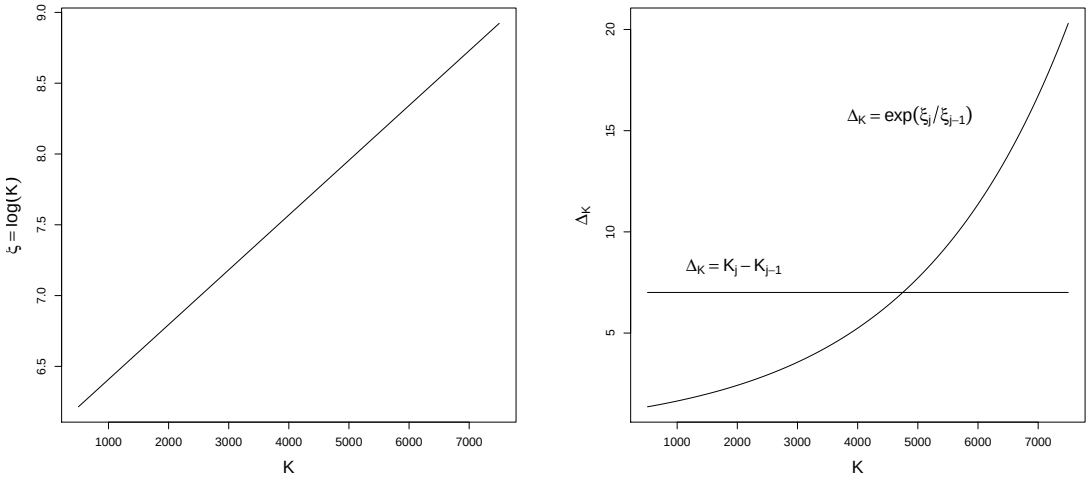

(a) Implications of the space coordinate transformation on the grid size.

(b) The step size for the original coordinate K when the transformed and the original grid is both uniform.

Figure 11: Logarithmic transformation of the space coordinate.

If the grid for the transformed coordinate ξ is equidistant, then the spacing in terms of the original coordinate K becomes denser for small values as depicted in figure 11(b). Thus, by choosing the boundaries K_{min} and K_{max} cleverly in proportion to the current spot s, is it possible to reduce the step size around the critical area $s = K_j$ compared to the uniform spacing.

The derivative of the transformation in terms of the new coordinate is given by:

$$\frac{d\exp(\xi)}{d\xi} = exp(\xi)$$

and the PDE in eqn. (16) written under the transformation is then given by[20]:

$$
\begin{aligned}
&-\frac{\partial C}{\partial \tau}(\tau,\xi)+\frac{\sigma^2(\tau+t,\exp(\xi))}{2}\frac{\exp(\xi)^2}{\exp(\xi)}\frac{\partial}{\partial \xi}\left(\frac{1}{\exp(\xi)}\frac{\partial C}{\partial \xi}(\tau,\xi)\right)=0\\
\Leftrightarrow\\
&-\frac{\partial C}{\partial \tau}(\tau,\xi)+\frac{\sigma^2(\tau+t,\exp(\xi))}{2}\frac{\exp(\xi)^2}{\exp(\xi)}\left(\frac{1}{\exp(\xi)}\frac{\partial^2 C}{\partial \xi^2}(\tau,\xi)-\frac{1}{\exp(\xi)}\frac{\partial C}{\partial \xi}(\tau,\xi)\right)=0\\
\Leftrightarrow\\
&-\frac{\partial C}{\partial \tau}(\tau,\xi)+\frac{1}{2}\sigma^2(\tau+t,\exp(\xi))\left(\frac{\partial^2 C}{\partial \xi^2}(\tau,\xi)-\frac{\partial C}{\partial \xi}(\tau,\xi)\right)=0
\end{aligned}
$$

Thus, the fully discretised implicit finite difference equation with the proxy's used in the calibration becomes:

$$
\left[1-\frac{1}{2}\Delta\tau_i\vartheta_i^2(\exp(\xi_j))\left(\delta_{\xi\xi}-\delta_\xi\right)\right]\hat{C}_{i,j}=\hat{C}_{i-1,j}\quad i=1,\ldots,n,\quad j=1,\ldots,m-1.
$$

where δ_y is the one-sided difference scheme for the first order derivative w.r.t. y given by:

$$
\delta_y f(x_i,y_j)=\frac{1}{\Delta y}\left(f(x_i,y_j)-f(x_i,y_j-\Delta y)\right)
$$

and the initial condition and the absorbing boundary conditions are given by:

$$
\begin{aligned}
\hat{C}_{0,j}&=(s-\exp(\xi_j))^+\quad j=0,\ldots,m.\\
\delta_{\xi\xi}\hat{C}_{i,0}=\delta_\xi\hat{C}_{i,0}=\delta_{\xi\xi}\hat{C}_{i,m}=\delta_\xi\hat{C}_{i,m}&=0\quad i=1,\ldots,n.
\end{aligned}
$$

The finite difference approximation to the local volatility parameter, (26), in this set-up becomes:

$$
\sigma^2(\tau+t,\exp(\xi))=2\frac{\frac{1}{\Delta\tau}\left(\hat{C}(\tau_l,K_j)-\hat{C}(\tau_{l-1},K_j)\right)}{\delta_{\xi\xi}\hat{C}(\tau,\xi)-\delta_\xi\hat{C}(\tau,\xi)}
$$

[20]See Tavella and Randall (2000, p. 157-159) for further details on the coordinate transformation procedure.

The implicit finite difference system of equations, (22), for the transformed coordinates is given by:

$$\mathbf{A}_i \cdot \hat{C}(\tau_i, \bar{\xi}) = \hat{C}(\tau_{i-1}, \bar{\xi}) \tag{39}$$

$\mathbf{A}_i$ is given below:

$$\mathbf{A}_i = \begin{bmatrix} 1 & 0 & 0 & 0 \\ -z_1^i\left(\frac{1}{\Delta\xi}+\frac{1}{2}\right) & 1+\frac{2}{\Delta\xi}z_1^i & -z_1^i\left(\frac{1}{\Delta\xi}-\frac{1}{2}\right) & 0 \\ \ddots & \ddots & \ddots & 0 \\ 0 & -z_{m-1}^i\left(\frac{1}{\Delta\xi}+\frac{1}{2}\right) & 1+\frac{2}{\Delta\xi}z_{m-1}^i & -z_{m-1}^i\left(\frac{1}{\Delta\xi}-\frac{1}{2}\right) \\ 0 & \cdots & 0 & 1 \end{bmatrix} \tag{40}$$

where the coefficients z_j^i are given by:

$$z_j^i = \frac{\vartheta_i(\exp(\xi_j))^2}{2}\frac{\Delta\tau_i}{\Delta\xi} \qquad j = 2, \ldots, m-1.$$

Remark that for this system there is a constraint on the step size: $\Delta\xi \leq 2$.

The implementation for the original coordinates is altered such that the underlying grid is given in terms of ξ instead of K. The optimal grid size and the constants used for this new grid has to be determined as in section 7.1. The log-transformed equivalent to table 1 is given in table 5.
Table 5 indicates that the appropriate boundaries for the spatial grid is given by:

$$\xi_{min} = 6.5 \qquad \xi_{max} = 9.0.$$

The upper bound could probably be lowered a bit without encountering oscillations.

As for the original coordinates, it can be seen in the table how a decrease in the constant Tol induces a significant increase in the fit between the observed call prices and the calculated prices. A reduction below $1e-10$ does not add further precision, thus this value is used in the remaining calculations.

One should keep in mind that this reduction of Tol increases the computational time by a factor of around 6. Hence, for practical purposes it might not be the optimal value for Tol. How coarse a grid and how *bad* a fit one can get away with i practice is discussed further below in section 7.3.

Sec's	0.21	0.29	0.4	1.73	3.39	9.69	213.12
Tol	1.00E-003	1.00E-003	1.00E-003	1.00E-010	1.00E-010	1.00E-010	1.00E-010
$\Delta\xi$	0.01	0.01	0.01	0.01	0.005	0.001	0.0001
ξ_{min}	7	6.5	6	6.5	6.5	6.5	6.5
ξ_{max}	8.5	9	9.5	9	9	9	9
τ_i	χ_i^2	χ_i^2	χ_i^2	χ_i^2	χ_i^2	χ_i^2	χ_i^2
0.025	2.50E-05	2.50E-05	1.62E-05	4.17E-28	1.08E-26	6.72E-25	1.81E-19
0.101	2.42E-27	3.03E-27	5.04E-27	3.96E-30	4.70E-28	2.13E-24	2.83E-22
0.197	3.76E-22	3.76E-22	1.95E-13	2.87E-29	2.24E-29	8.02E-25	7.28E-23
0.274	1.84E-27	6.22E-29	1.07E-28	5.86E-28	7.96E-28	1.96E-23	1.80E-20
0.523	6.50E-30	2.98E-27	5.31E-30	7.79E-29	1.03E-28	3.98E-25	2.69E-22
0.772	5.46E-29	5.49E-27	1.32E-27	6.65E-30	5.74E-28	2.37E-23	2.36E-19
1.769	2.45E-21	2.70E-21	9.59E-21	1.57E-28	1.84E-27	7.01E-25	5.68E-19
2.267	7.60E-28	4.18E-29	1.17E-28	3.33E-30	9.63E-27	4.50E-24	2.19E-22
2.784	4.60E-04	1.82E-27	4.62E-26	6.38E-27	6.04E-26	7.86E-24	4.41E-19
3.781	5.17E-04	2.79E-06	4.85E-06	3.62E-08	9.61E-09	2.91E-08	3.12E-08
4.778	8.22E-06	8.92E-05	8.93E-05	3.65E-06	3.91E-06	3.60E-06	3.51E-06
5.774	2.71E-12	4.80E-26	3.23E-26	1.85E-28	4.35E-27	1.81E-25	1.07E-21
Avg χ_i^2	8.42E-005	9.75E-006	9.20E-06	3.07E-07	3.27E-07	3.02E-07	2.95E-07
Avg # iter	5.17	4.75	5.08	38.08	42.50	26.42	58.67

Table 5: Values of χ_i^2 for different choices of constants for the implementation described in section 5 with log transformed space coordinates. The results is based on the data in table 8.

The picture regarding the step size is equivalent to the case for the original space coordinates and the steady state for volatility levels seems to occur for sizes below 0.005. Again, this level can probably be increased in practice.

The χ_i^2 values in table 5 reveals that the critical areas is still a problem for the log transformed system although the average number of iterations for each observed maturity is somewhat higher. Thus, these values are removed from the data in order to get reliable results. The equivalent to table 3 is given in table 6.

The removal of the *bad* observations decreases the computational time by approximately a factor 5 as the number of iterations is heavily decreased. But the χ_i^2 values for the critical maturities 3.718 and 4.778 suggest that a higher number of iterations for the *clean* version would probably give a better fit. This problem is most likely (again) due to the lack of robustness in the implementation of the optimization procedure.

The calibrated proxy levels a_{ij} for these maturities around the remaining observable strike levels is however sensible as can be seen in table 7. Remark that these volatility levels deviates a bit from the levels given in table 10 that where calibrated using the original coordinates. As the calibrations is

	Org		Clean	
Sec's	3.39		0.7	
τ_i	χ_i^2	# iter	χ_i^2	# iter
0.025	1.08E-026	9	1.07564E-026	9
0.101	4.7E-028	7	4.7006E-028	7
0.197	2.24E-029	7	2.23643E-029	7
0.274	7.96E-028	7	7.96012E-028	7
0.523	1.03E-028	7	1.02729E-028	7
0.772	5.74E-028	7	5.73696E-028	7
1.769	1.84E-027	8	1.8402E-027	8
2.267	9.63E-027	6	9.63496E-027	6
2.784	6.04E-026	7	6.03606E-026	7
3.781	9.61E-09	39	0.00462445	8
4.778	3.91E-06	399	0.00622527	7
5.774	4.35E-027	7	1.09909E-027	7

Table 6: The number of iterations, the χ_i^2 values and the run-time in seconds for the log transformed space coordinates based on data with and without observations: $(3.718, 95.29)$ and $(4.778, 58.64)$. The constants are set to: $\Delta\xi$ =0.05, $\xi_{min} = 6.5$,$\xi_{max} = 9$ and $Tol = 1e-10$.

carried out in two different grid-and-constants settings, one cannot expect a perfect agreement between these versions.

The calibration accuracy[21], discussed in the previous section, are equivalent to the ones reported for the original coordinates - in table 4 - for the accuracy level that can be achieved using 'R'.

The local volatility surface obtained for these transformed coordinates is given in figure 12. Remark that the local volatility surface for the highest strike levels does not bend upwards as seen in figure 10 for the original grid.

Thus, the numerical examples above illustrates that the local volatility surface can be calibrated must faster for the same level of accuracy using logarithmic transformed coordinates in the underlying grid.

[21] Calibration accuracy for the data without observations $(3.718, 95.29)$ and $(4.778, 58.64)$, for constants: $\Delta\xi$ =0.05, $\xi_{min} = 6.5$,$\xi_{max} = 9$ and $Tol = 1e-10$.

	0.025	0.101	0.197	0.274	0.523	0.772	1.769	2.267	2.784	3.781	4.778	5.774
51.31									62.29	50.18		
58.64									39.85	42.45		
65.97									42.87	31.21	42.55	
73.3									38.62	46.99	39.83	
76.97				54.75	40.42	41.07	38.94					
80.63				34.7	35.26	37.71	31.73	35.22	28.80	31.65	29.07	46.78
84.3				37.29	34.5	29.39	42.16					
86.13	22.58											
87.96	23.98	30.8	34.40	31.08	32.04	35.95	23.99	27.20	33.49	25.22	33.77	34.56
89.79	21.46	29.84	32									
91.63	21.82	28.62	28.51	29.22	29.72	26.33	35.25					
93.46	21.45	30.37	27.34									
95.29	22.54	28.43	24.91	26.09	26.74	29.61	24.48	26.1	29.02		31.81	30.02
97.12	25.21	26.81	25.68									
98.96	31.1	26.79	22.52	24.23	24.67	22.94	24.53					
100.79	26.73	23.75	22.21									
102.62	17.81	21.94	20.53	20.76	22.05	22.68	33.46	21.18	22.76	37.83	20.24	27.89
104.45	13.93	19.5	19.41									
106.29	10.78	17.05	19.35	18.84	19.98	19.73	20.98					
108.12	9.993	14.74	18.28									
109.95	7.207	14.36	14.82	17.78	17.98	18.66	23.44	21.16	25.29	17.79	27.05	26.46
111.78	-4.632	11.19	15.56									
113.62				15.07	16.11	17.46	18.99					
117.28				16.93	14.26	15.75	20.21	17.36	18.43	29.01	17.38	25.28
120.95				13.47	13.27	15.98	18.26					
124.61				14.01	12.57	13.16	15.09		23.01	15.20	25.77	22.34
131.94									17.74	25.77	19.01	22.83
139.27									24.73	16.59	18.43	19.12
146.6									10.06	18.36	17.16	

Table 7: Volatility levels: a_{ij}, for the data in table 8 without observations: $(3.718, 95.29)$ and $(4.778, 58.64)$, for constants: $\Delta\xi$ =0.05, $\xi_{min} = 6.5$,$\xi_{max} = 9$ and $Tol = 1e-10$.

7.3 How low can you go?

The smoothness of the calibrated call surface is essential for obtaining a nice local volatility surface without any discontinuities or spikes. The surfaces generated by traditional techniques are mentioned in *Risk awards 2012 - Quants of the year* - magazine staff (2012), as:

> *The poor quality of these surfaces was the dirty secret of the industry...*

The local volatility surface generated by Andreasen and Huge's method displayed in figure 10 and 12 have no spikes and no *black* holes. Thus, these surfaces are smooth enough for practical purposes.

As the computational cost is of great importance in practice, it is an obvious question to ask how the structure of the call- and local volatility- surfaces respond to increases in the step size of the underlying grid.

The call surface for the *base* case is displayed from different angles in figure 13, recall that this surface could be calibrated in 0.7 seconds of CPU time.
To get a better view of the smoothness of these call prices, a 2D plot of the call prices as a function of the time-to-maturity for a couple of strike levels is

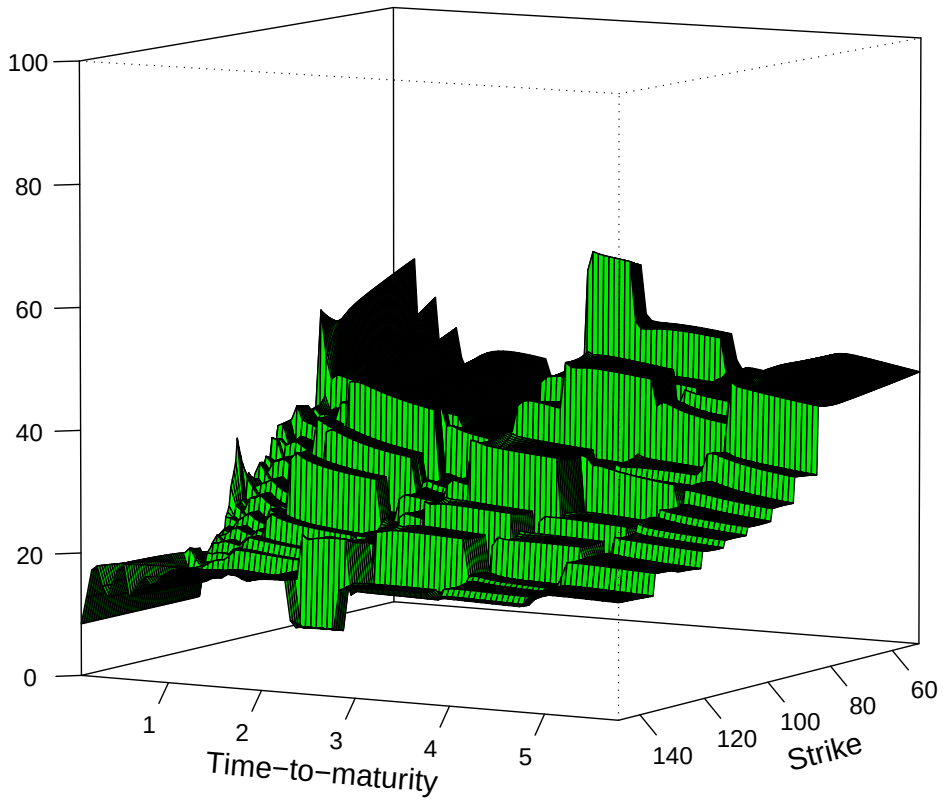

Figure 12: The local volatility surface calibrated to the data in table 8 without observations $(3.718, 95.29)$ and $(4.778, 58.64)$ for constants:$\Delta\xi$ =0.05, $\xi_{min} = 6.5$,$\xi_{max} = 9$, $\Delta T \approx 0.06$ and $Tol = 1e - 10$.

given in figure 14. The *eyeball* smoothness of the call prices is almost identical when the number of time steps is increased to 500 or decreased to 75, 50 or 25. The computational time is almost unaltered for different choices of step sizes in the time direction.

This structure also seems to remain unchanged when the step size is increased to: $\Delta\xi = 0.01$. This step size corresponds to a step size for the original

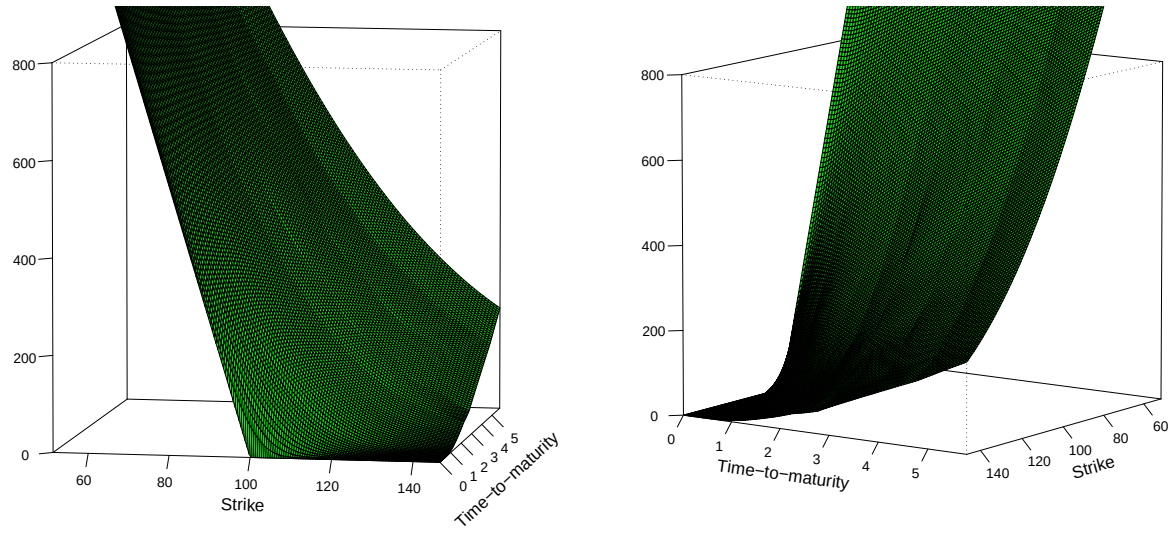

Figure 13: The call surface calibrated to the data in table 8 without observations $(3.718, 95.29)$ and $(4.778, 58.64)$ for constants:$\Delta\xi = 0.005$, $\xi_{min} = 6.5$,$\xi_{max} = 9$, $\Delta T \approx 0.06$ and $Tol = 1e-10$.

coordinate by $\Delta K_i = 6$ for the lower end of the spatial grid and $\Delta K_i > 30$ for the high end. The calibrated local volatility surface for this grid is given in figure 15.

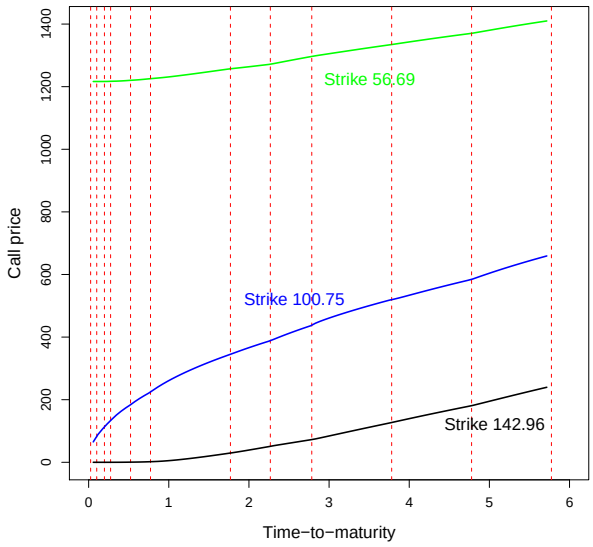

Figure 14: The call prices as a function of the time to maturity for three strike levels. Constants are set to:$\Delta\xi = 0.005$, $\xi_{min} = 6.5$,$\xi_{max} = 9$, $\Delta T \approx 0.06$ and $Tol = 1e - 10$.

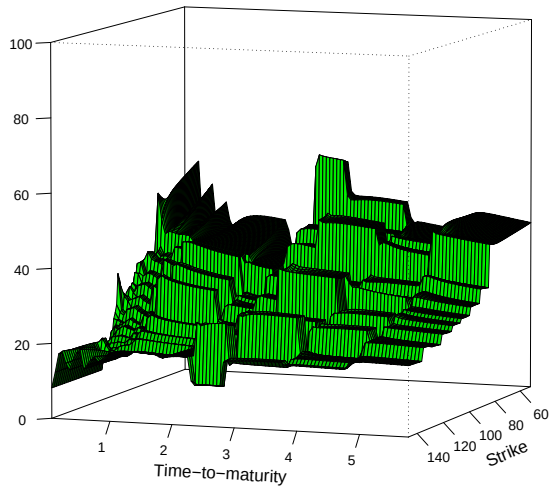

Figure 15: The local volatility surface. Constants are set to:$\Delta\xi$ =0.01, $\xi_{min} = 6.5$,$\xi_{max} = 9$, $\Delta T \approx 0.06$ and $Tol = 1e - 10$.

7.4 Crank it up

If one assumes absorbing boundaries, as in for the implementations above, this yields a system of equation:

$$\mathbf{A}_i \cdot \hat{C}(\tau_i, \bar{\xi}) = \mathbf{B}_i \hat{C}(\tau_{i-1}, \bar{\xi})$$

where $\mathbf{A}_i$ is given as in eqn. (40) with coefficients z_j^i given by:

$$z_j^i = \frac{\vartheta_i(\exp(\xi_j))^2}{4} \frac{\Delta\tau_i}{\Delta\xi} \qquad j = 2, \ldots, m-1.$$

and $\mathbf{B}_i$ is also given as the matrix in eqn. (40) with coefficients z_j^i given by:

$$z_j^i = -\frac{\vartheta_i(\exp(\xi_j))^2}{4} \frac{\Delta\tau_i}{\Delta\xi} \qquad j = 2, \ldots, m-1.$$

As briefly mentioned in section 5.1.1, is the Crank-Nicolson method given as the *average* of the implicit method:

$$-\frac{\hat{C}_{i,j} - \hat{C}_{i-1,j}}{\Delta\tau_i} + \frac{1}{2}\vartheta_i^2(\exp(\xi_j))\left(\delta_{\xi\xi} - \delta_\xi\right)\hat{C}_{i,j} = 0$$

and the explicit:

$$-\frac{\hat{C}_{i,j} - \hat{C}_{i-1,j}}{\Delta\tau_i} + \frac{1}{2}\vartheta_i^2(\exp(\xi_j))\left(\delta_{\xi\xi} - \delta_\xi\right)\hat{C}_{i-1,j} = 0$$

Thus, the finite difference equation for this method is given by:

$$-\frac{\hat{C}_{i,j} - \hat{C}_{i-1,j}}{\Delta\tau_i} + \frac{1}{4}\vartheta_i^2(\exp(\xi_j))\left(\delta_{\xi\xi} - \delta_\xi\right)\hat{C}_{i,j} + \frac{1}{4}\vartheta_i^2(\exp(\xi_j))\left(\delta_{\xi\xi} - \delta_\xi\right)\hat{C}_{i-1,j} = 0$$

$\Leftrightarrow$

$$\left[1 - \frac{\Delta\tau_i}{4}\vartheta_i^2(\exp(\xi_j))\left(\delta_{\xi\xi} - \delta_\xi\right)\right]\hat{C}_{i,j} = \left[1 + \frac{\Delta\tau_i}{4}\vartheta_i^2(\exp(\xi_j))\left(\delta_{\xi\xi} - \delta_\xi\right)\right]\hat{C}_{i-1,j}$$

with boundary conditions as for the logarithmic implementation above.

When this change in the finite difference part of the method is implemented, this results in a call surface where there seems to be a line of oscillations running through. But this is hard to depict on as small graph, as can be stated by looking at figure 16.

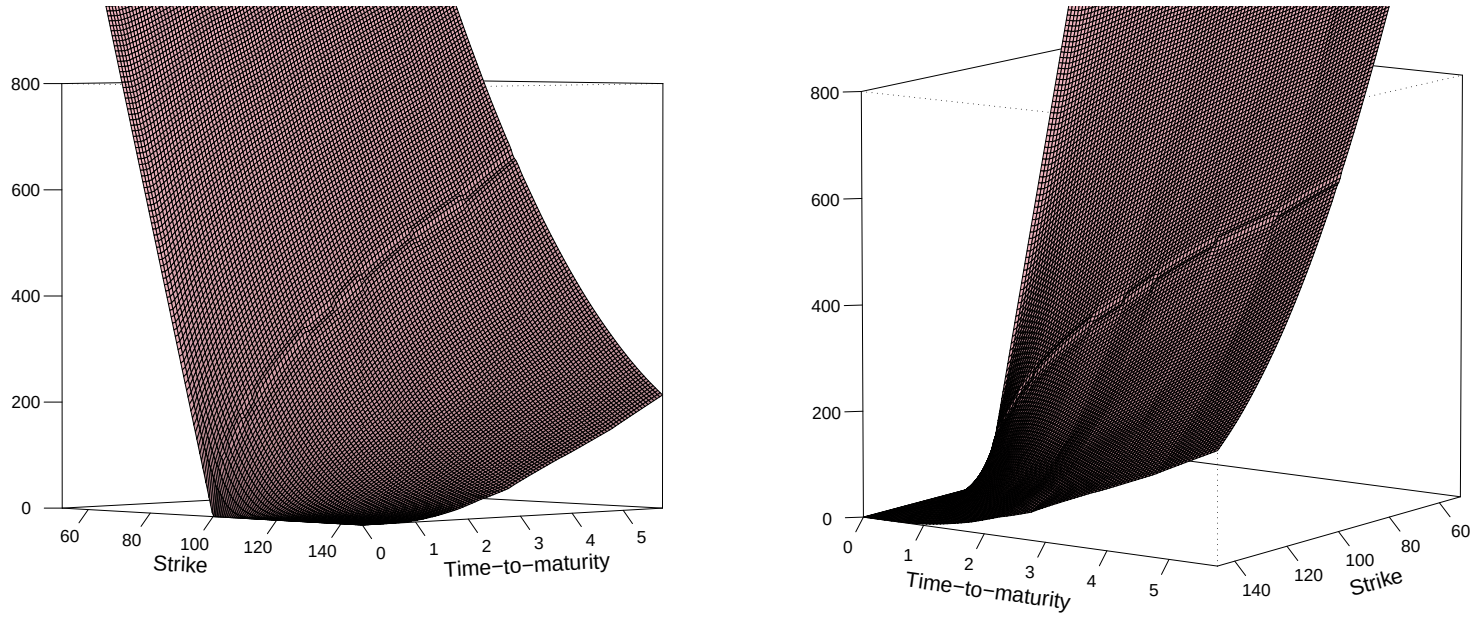

Figure 16: The Crank-Nicolson call surface calibrated to the data in table 8 without observations $(3.718, 95.29)$ and $(4.778, 58.64)$ for constants:$\Delta\xi = 0.005$, $\xi_{min} = 6.5$,$\xi_{max} = 9$, $\Delta T \approx 0.06$ and $Tol = 1e-10$

The 2D plot for the Crank-Nicolson implementation equivalent to figure 14 is given in figure 17.

This figure 17 reveals as expected some oscillations around the strike level equal to the spot price for the underlying SX5E index. A zoom at this area is displayed in figure 18.
These oscillations causes discontinuities in the local volatility function around this area. Thus, the method presented by Andreasen and Huge cannot be used with a Crank-Nicolson finite difference scheme, just as could be expected from the derivations in section 6.

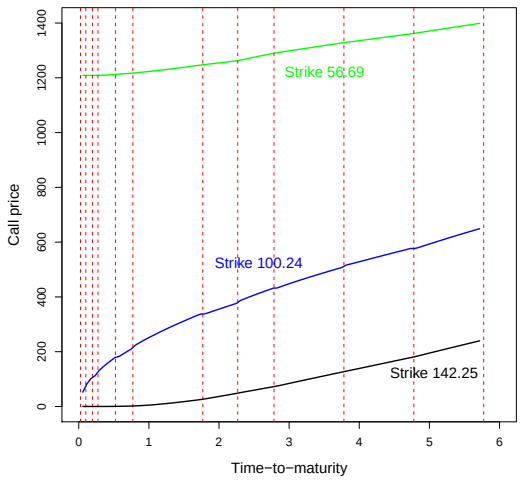

Figure 17: The call prices as a function of the time to maturity for three strike levels. Constants are set to:$\Delta\xi$ =0.01, $\xi_{min} = 6.5$,$\xi_{max} = 9$, $\Delta T \approx 0.06$ and $Tol = 1e - 10$.

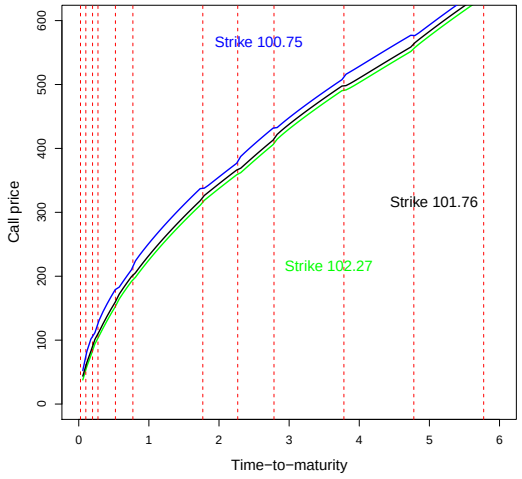

Figure 18: The call prices as a function of the time to maturity for three strike levels. Constants are set to:$\Delta\xi$ =0.01, $\xi_{min} = 6.5$,$\xi_{max} = 9$, $\Delta T \approx 0.06$ and $Tol = 1e - 10$.

8 Conclusion and future work

This thesis has considered the calibration method for the local volatility model presented by Andreasen and Huge in their article *Volatility Interpolation* from 2011.

It was initially examined how this method relates to the existing research within this area and which components of the method that could be recognized from other articles.

The procedure and the implementation where then described in in detail. The two main ingredients of the implementation is the implicit finite difference solver - which is a well-known method and simple to use - and the standard Levenberg-Marquardt optimization algorithm. Thus, even though the method is sophisticated, the main ingredients of the implementation is recognisable for many practitioners.

The (discrete) surface of call prices calibrated by this method where shown to be arbitrage free, both for the semi-discrete and the fully discrete case. Thus, the greed for convergence, and thereby absence of arbitrage, seen in similar approaches, is not a priority when using this technique.

It could also be noticed that the absence of arbitrage depends on the piecewise time-independent volatility proxy and on the structure of the implicit finite difference scheme. That is why the alternative Crank-Nicolson scheme implemented in section 7 gave some ugly results for the strike level near the current spot price.

The other numerical experiments carried out for both the original and the logarithmic transformed coordinates seemed to be robust to changes in the *constants* and produced sufficiently smooth call- and local volatility- surfaces in a split second if it was provided with good data.

Possible extension of this method have been proposed in the article by magazine staff (2012). These include adding jumps and expanding the method to handle other underlying assets besides equity.

On the more technical side, a simple improvement could be to place the observed strike levels on the grid, such that linear interpolation for these becomes unnecessary. Another obvious improvement of the speed would be to apply parallelism to the interpolating part of the algorithm.

There are no fundamental laws handed down from God on clay tablets. I think there is still a tendency to see the world through models, forgetting they are only as good as their implementation.

- Jesper Andreasen 2012.

References

Leif B. G. Andersen and Rupert Brotherton-Ratcliffe. The equity option volatility smile: an implicit finite-difference approach. *The Journal of Computational Finance*, 1(2):5–36, Winter 1997/98.

Jesper Andreasen. *Essays on contingent Claim Pricing*. PhD thesis, University of Aarhus, 1997.

Jesper Andreasen. Finite difference methods for finance problems. The Danish Doctoral School of Finance, March 2011.

Jesper Andreasen and Brian N. Huge. Volatility interpolation. *Risk Magazine*, March 2011. `http://ssrn.com/paper=1694972`.

Tomas Björk. *Arbitrage Theory in Continuous Time*. Oxford University Press, 3rd edition, 2009.

C. Blanco. Volatility smiles, surfaces and option prices. `http://fea.com/resources/articles.asp`, November 2002.

Peter Carr. Option pricing using integral transforms. `http://www.math.nyu.edu/research/carrp/papers/pdf/integtransform.pdf`. Presentation.

Peter Carr. Local variance gamma. Working paper - Bloomberg LP, January 2008.

Peter Carr and Dilip B. Madan. A note on suffiecient conditions for no arbitrage. *Finance Research Letters*, (2):125–130, 2005.

Thomas F. Coleman, Yuying Li, and Arun Verma. Reconstructing the unknown local volatility function. *Journal of Computational Finance*, 2:77–102, 1998.

Daniel J. Duffy. *Financial instrument pricing using C++*. John Wiley & Sons, Ltd, 2004.

Bruno Dupire. Pricing and hedging with smiles. Can be downloaded from: `http://www.globalriskguard.com/virtual-library/derivatives/`, April 1993.

Bruno Dupire. Pricing with a smile. *Risk*, 7(1):18–20, January 1994.

Jim Gatheral. *The Volatility Surface - a practitioner's guide*. John Wiley & Sons, Inc., 2006.

John C. Hull. *Options, futures and other derivatives*. Pearson Prentice Hall, 7th edition, 2008.

Jens Carsten Jackwerth and Mark Rubinstein. Recovering the probability distributions from option prices. *The Journal of Finance*, 51(5):1611–1631, Dec. 1996.

Risk magazine staff. Risk awards 2012 - quants of the year: Jesper andreasen and brian huge, danske bank. `http://www.risk.net/risk-magazine/feature/2133160/quants-jesper-andreasen-brian-huge-danske-bank`, January 2012.

Claus Munk. Introduction to the numerical solution of partial differential equations in finance. October 2007.

planetmath.org. M-matrix.

William H. Press, Saoul A. Teukolsky, William T. Vetterling, and Brian P. Flannery. *Numerical recipes - the art of scientific computing*. Cambridge University Press, 3rd edition, 2007.

Artur Sepp. Using sabr model to produce smooth local volatility surfaces. Working paper, Merrill Lynch, 2007.

Domingo Tavella and Curt Randall. *Pricing financial instruments - The finite difference method*. John Wiley & Sons, Inc., 2000.

wikipedia. Derivative (finance). `http://en.wikipedia.org/wiki/Derivative_(finance)`.

the free encyclopedia Wikipedia. Z-matrix (mathematics).

A Additional data

Table 8: Implied Black Scholes volatilities for European-style options on the SX5E index. Expiries range from two weeks to a little under six years and strikes range from $50-146\%$ of current spot 2772.70. Data is of March 1, 2010, and originally given in Andreasen and Huge (2011).

	0.025	0.101	0.197	0.274	0.523	0.772	1.769	2.267	2.784	3.781	4.778	5.774
51.31	0.00	0.00	0.00	0.00	0.00	0.00	0.00	0.00	33.66	32.91	0.00	0.00
58.64	0.00	0.00	0.00	0.00	0.00	0.00	0.00	0.00	31.78	31.29	30.08	0.00
65.97	0.00	0.00	0.00	0.00	0.00	0.00	0.00	0.00	30.19	29.76	29.75	0.00
73.3	0.00	0.00	0.00	0.00	0.00	0.00	0.00	0.00	28.63	28.48	28.48	0.00
76.97	0.00	0.00	0.00	32.62	30.79	30.01	28.43	0.00	0.00	0.00	0.00	0.00
80.63	0.00	0.00	0.00	30.58	29.36	28.76	27.53	27.13	27.11	27.11	27.22	28.09
84.3	0.00	0.00	0.00	28.87	27.98	27.50	26.66	0.00	0.00	0.00	0.00	0.00
86.13	33.65	0.00	0.00	0.00	0.00	0.00	0.00	0.00	0.00	0.00	0.00	0.00
87.96	32.16	29.06	27.64	27.17	26.63	26.37	25.75	25.55	25.80	25.85	26.11	26.93
89.79	30.43	27.97	26.72	0.00	0.00	0.00	0.00	0.00	0.00	0.00	0.00	0.00
91.63	28.80	26.90	25.78	25.57	25.31	25.19	24.97	0.00	0.00	0.00	0.00	0.00
93.46	27.24	25.90	24.89	0.00	0.00	0.00	0.00	0.00	0.00	0.00	0.00	0.00
95.29	25.86	24.88	24.05	24.07	24.04	24.11	24.18	24.10	24.48	24.69	25.01	25.84
97.12	24.66	23.90	23.29	0.00	0.00	0.00	0.00	0.00	0.00	0.00	0.00	0.00
98.96	23.58	23.00	22.53	22.69	22.84	22.99	23.47	0.00	0.00	0.00	0.00	0.00
100.79	22.47	22.13	21.84	0.00	0.00	0.00	0.00	0.00	0.00	0.00	0.00	0.00
102.62	21.59	21.40	21.23	21.42	21.73	21.98	22.83	22.75	23.22	23.84	23.92	24.86
104.45	20.91	20.76	20.69	0.00	0.00	0.00	0.00	0.00	0.00	0.00	0.00	0.00
106.29	20.56	20.24	20.25	20.39	20.74	21.04	22.13	0.00	0.00	0.00	0.00	0.00
108.12	20.45	19.82	19.84	0.00	0.00	0.00	0.00	0.00	0.00	0.00	0.00	0.00
109.95	20.25	19.59	19.44	19.62	19.88	20.22	21.51	21.61	22.19	22.69	23.05	23.99
111.78	19.33	19.29	19.20	0.00	0.00	0.00	0.00	0.00	0.00	0.00	0.00	0.00
113.62	0.00	0.00	0.00	19.02	19.14	19.50	20.91	0.00	0.00	0.00	0.00	0.00
117.28	0.00	0.00	0.00	18.85	18.54	18.88	20.39	20.58	21.22	21.86	22.23	23.21
120.95	0.00	0.00	0.00	18.67	18.11	18.39	19.90	0.00	0.00	0.00	0.00	0.00
124.61	0.00	0.00	0.00	18.71	17.85	17.93	19.45	0.00	20.54	21.03	21.64	22.51
131.94	0.00	0.00	0.00	0.00	0.00	0.00	0.00	0.00	19.88	20.54	21.05	21.90
139.27	0.00	0.00	0.00	0.00	0.00	0.00	0.00	0.00	19.30	20.02	20.54	21.35
146.6	0.00	0.00	0.00	0.00	0.00	0.00	0.00	0.00	18.49	19.64	20.12	0.00

Table 9: Call prices for European-style options on the SX5E index. Expiries range from two weeks to a little under six years, strikes range from $1422 - 4064$ and the current spot is 2772.70. Data is of March 1, 2010, and given in Andreasen and Huge (2011).

	0.025	0.101	0.197	0.274	0.523	0.772	1.769	2.267	2.784	3.781	4.778	5.774
1422.67	0.00	0.00	0.00	0.00	0.00	0.00	0.00	0.00	1412.47	1444.42	0.00	0.00
1625.91	0.00	0.00	0.00	0.00	0.00	0.00	0.00	0.00	1237.37	1278.28	1305.98	0.00
1829.15	0.00	0.00	0.00	0.00	0.00	0.00	0.00	0.00	1071.39	1119.64	1168.42	0.00
2032.39	0.00	0.00	0.00	0.00	0.00	0.00	0.00	0.00	913.69	971.77	1025.98	0.00
2134.15	0.00	0.00	0.00	649.81	670.37	692.44	770.38	0.00	0.00	0.00	0.00	0.00
2235.63	0.00	0.00	0.00	553.51	579.80	605.68	692.47	727.80	765.35	830.77	890.94	962.24
2337.39	0.00	0.00	0.00	460.13	492.40	521.83	617.58	0.00	0.00	0.00	0.00	0.00
2388.13	384.68	0.00	0.00	0.00	0.00	0.00	0.00	0.00	0.00	0.00	0.00	0.00
2438.87	334.08	342.85	358.15	370.78	409.39	442.94	545.51	585.97	630.24	700.37	766.57	840.55
2489.61	283.65	295.88	313.89	0.00	0.00	0.00	0.00	0.00	0.00	0.00	0.00	0.00
2540.63	233.34	250.17	270.92	286.92	331.36	368.07	478.36	0.00	0.00	0.00	0.00	0.00
2591.37	184.21	206.84	230.26	0.00	0.00	0.00	0.00	0.00	0.00	0.00	0.00	0.00
2642.11	137.06	166.08	192.10	211.13	260.00	299.55	415.02	458.49	506.43	581.45	650.71	727.25
2692.85	93.84	128.76	157.04	0.00	0.00	0.00	0.00	0.00	0.00	0.00	0.00	0.00
2743.86	57.04	95.65	125.01	145.54	196.33	236.61	356.72	0.00	0.00	0.00	0.00	0.00
2794.60	29.46	67.62	97.01	0.00	0.00	0.00	0.00	0.00	0.00	0.00	0.00	0.00
2845.34	12.41	45.32	73.18	92.58	141.98	181.69	303.87	346.75	396.10	479.34	543.70	623.89
2896.09	4.11	28.56	53.55	0.00	0.00	0.00	0.00	0.00	0.00	0.00	0.00	0.00
2947.10	1.09	16.88	38.03	53.84	97.68	134.74	254.52	0.00	0.00	0.00	0.00	0.00
2997.84	0.24	9.39	26.12	0.00	0.00	0.00	0.00	0.00	0.00	0.00	0.00	0.00
3048.58	0.04	5.02	17.23	28.69	63.81	96.67	211.02	253.93	303.32	381.75	450.98	530.94
3099.32	0.00	2.46	11.20	0.00	0.00	0.00	0.00	0.00	0.00	0.00	0.00	0.00
3150.34	0.00	0.00	0.00	13.89	39.36	66.82	172.36	0.00	0.00	0.00	0.00	0.00
3251.82	0.00	0.00	0.00	6.63	23.08	44.59	139.42	178.83	225.34	302.04	368.83	448.15
3353.58	0.00	0.00	0.00	2.92	13.02	28.90	111.16	0.00	0.00	0.00	0.00	0.00
3455.06	0.00	0.00	0.00	1.30	7.22	17.97	87.53	0.00	165.67	233.26	301.42	375.25
3658.30	0.00	0.00	0.00	0.00	0.00	0.00	0.00	0.00	118.24	181.55	242.73	312.27
3861.54	0.00	0.00	0.00	0.00	0.00	0.00	0.00	0.00	82.42	138.27	193.98	257.99
4064.78	0.00	0.00	0.00	0.00	0.00	0.00	0.00	0.00	53.07	105.25	154.39	0.00

	0.025	0.101	0.197	0.274	0.523	0.772	1.769	2.267	2.784	3.781	4.778	5.774
51.31									59.06	45.77		
58.64									39.75	43.16		
65.97									42.76	31.21	41.16	
73.3									38.78	47.02	40.25	
76.97				55.36	40.47	41.06	39					
80.63				34.97	35.44	38.31	31.62	35.19	28.85	31.79	29.12	45.46
84.3				37.5	34.62	29.31	43.81					
86.13	21.02											
87.96	24.23	30.84	34.45	31.42	32.24	35.89	24.3	27.24	33.52	25.23	33.74	34.76
89.79	21.63	30.04	32.45									
91.63	21.89	28.57	28.74	29.31	29.84	26.42	34.84					
93.46	21.38	30.31	27.56									
95.29	22.27	28.7	24.96	26.22	26.89	29.86	24.76	26.13	29.12		31.98	30.06
97.12	24.40	26.95	25.89									
98.96	30.41	27	23.16	24.45	24.88	23.27	24.3					
100.79	27.43	23.75	22.06									
102.62	18.78	22.22	20.82	20.88	22.14	22.70	33.49	21.17	22.69	39.43	20.12	27.93
104.45	13.82	19.49	19.3									
106.29	11.31	17.38	19.42	18.86	20.03	19.80	21.04					
108.12	9.878	14.56	18.45									
109.95	8.123	14.82	15.38	17.97	18.15	18.77	23.64	21.24	25.34	17.98	26.95	26.54
111.78	-4.917	11.31	15.44									
113.62				15.19	16.19	17.51	19.17					
117.28				16.95	14.3	15.77	20.09	17.40	18.53	28.29	17.51	25.24
120.95				13.52	13.29	16.21	18.57					
124.61				14.08	12.63	13.31	15.19		23.06	15.16	25.78	22.52
131.94									17.73	25.76	19.17	21.63
139.27									25.6	16.25	17.64	28.3
146.6									10.81	22.22	26.05	

Table 10: Volatility levels: a_{ij}, for the data in table 8 where observations ($\tau = 3.718, K = 95.29$) and ($\tau = 4.778, K = 58.64$) have been removed. The constants are set to: ΔK =1, $K_{min} = 422$,$K_{min} = 5064$ and $tol = 1e - 10$.